Altered oligomeric states in pathogenic ALS2 variants associated with juvenile motor neuron diseases cause loss of ALS2-mediated endosomal function

Received for publication, May 7, 2018, and in revised form, September 13, 2018 Published, Papers in Press, September 17, 2018, DOI 10.1074/jbc.RA118.003849

Kai Sato[‡], Asako Otomo[‡§¶], Mahoko Takahashi Ueda[¶], Yui Hiratsuka[‡], Kyoko Suzuki-Utsunomiya[‡], Junya Sugiyama[‡], Shuji Murakoshi[‡], Shun Mitsui[‡], Suzuka Ono[‡], So Nakagawa[‡§¶], Hui-Fang Shang[‖], and Shinji Hadano[‡§1]**

*From the [‡]Department of Molecular Life Sciences, Tokai University School of Medicine, 143 Shimokasuya, Isehara, Kanagawa 259-1193, Japan, [§]The Institute of Medical Sciences, Tokai University, Isehara, Kanagawa 259-1193, Japan, [¶]Micro/Nano Technology Center, Tokai University, Hiratsuka, Kanagawa 259-1292, Japan, [‖]Department of Neurology, West China Hospital, Sichuan University, Chengdu, Sichuan 610041, China, and **Research Center for Brain and Nervous Diseases, Tokai University Graduate School of Medicine, Isehara, Kanagawa 259-1193, Japan*

Edited by Karen G. Fleming

Familial amyotrophic lateral sclerosis type 2 (ALS2) is a juvenile autosomal recessive motor neuron disease caused by the mutations in the *ALS2* gene. The *ALS2* gene product, ALS2/alsin, forms a homophilic oligomer and acts as a guanine nucleotide–exchange factor (GEF) for the small GTPase Rab5. This oligomerization is crucial for both Rab5 activation and ALS2-mediated endosome fusion and maturation in cells. Recently, we have shown that pathogenic missense ALS2 mutants retaining the Rab5 GEF activity fail to properly localize to endosomes via Rac1-stimulated macropinocytosis. However, the molecular mechanisms underlying dysregulated distribution of ALS2 variants remain poorly understood. Therefore, we sought to clarify the relationship between intracellular localization and oligomeric states of pathogenic ALS2 variants. Upon Rac family small GTPase 1 (Rac1) activation, all mutants tested moved from the cytosol to membrane ruffles but not to macropinosomes and/or endosomes. Furthermore, most WT ALS2 complexes were tetramers. Importantly, the sizes of an ALS2 complex carrying missense mutations in the N terminus of the regulator of chromosome condensation 1–like domain (RLD) or in-frame deletion in the pleckstrin homology domain were shifted toward higher molecular weight, whereas the C-terminal vacuolar protein sorting 9 (VPS9) domain missense mutant existed as a smaller dimeric or trimeric smaller form. Furthermore, *in silico* mutagenesis analyses using the RLD protein structure in conjunction with a cycloheximide chase assay *in vitro* disclosed that these missense mutations led to a decrease in protein stability. Collectively, disorganized higher structures of ALS2 variants might explain their impaired endosomal localization and the stability, leading to loss of the ALS2 function.

Mutations in the *ALS2* gene account for a number of autosomal recessive juvenile-onset motor neuron diseases (MNDs),[2] including ALS type 2 (ALS2), juvenile primary lateral sclerosis, and infantile-onset ascending hereditary spastic paralysis (IAHSP). These MNDs are characterized by a selective and progressive degeneration of motor neurons, particularly the upper motor neurons (1–3), indicating that the *ALS2* gene and its gene product, ALS2 (aka alsin), play crucial roles in the maintenance and/or survival of motor neurons (4, 5).

ALS2 is a 184-kDa protein of 1657 amino acid residues (aa) that comprises three predicted guanine nucleotide–exchange factor (GEF) domains as follows: the N-terminal regulator of chromosome condensation 1–like domain (RLD) (6); the central Dbl-homology and pleckstrin-homology (DH/PH) domain (7); and the C-terminal vacuolar protein sorting 9 (VPS9) domain (Fig. S1) (8). In addition, eight consecutive membrane occupation and recognition nexus (MORN) motifs (9) that are related to membrane binding are noted in the region between DH/PH and VPS9 domains. Indeed, it has been shown that ALS2 acts as a GEF for the small GTPase Rab5 via the C-terminal MORN/VPS9 domain and modulates endosome fusion and trafficking by activating Rab5 (10). Furthermore, the activation of Rac family small GTPase 1 (Rac1) results in a drastic redistribution of ALS2 from the cytosol to membrane compartments, thereby inducing endosome enlargement in an ALS2-mediated Rab5 GEF activity-dependent manner (11).

This work was supported by Japanese Society for Promotion of Science Grants 26290018 and 24650189 (to S. H.) and in part by the National Natural Science Foundation of China (to H.-F. S.) and JSPS Bilateral Joint Research Project (to S. H.). The authors declare that they have no conflicts of interest with the contents of this article.

This article contains Figs. S1–S9 and Tables S1–S2.

[1] To whom correspondence should be addressed: Dept. of Molecular Life Sciences, Tokai University School of Medicine, 143 Shimokasuya, Isehara, Kanagawa 259-1193, Japan. Tel.: 81-463-91-5095; E-mail: shinji@is.icc.u-tokai.ac.jp.

[2] The abbreviations used are: MND, motor neuron disease; ALS, amyotrophic lateral sclerosis; ALS2, amyotrophic lateral sclerosis type 2; CHX, cycloheximide; DH/PH, Dbl-homology/pleckstrin homology; EEA1, early endosome autoantigen 1; GEF, guanine nucleotide–exchange factor; GST, glutathione *S*-transferase; HRP, horseradish peroxidase; IAHSP, infantile-onset ascending hereditary spastic paralysis; MORN, membrane occupation and recognition nexus; NGS, normal goat serum; PI, phosphatidylinositol; PIP, phosphoinositide phosphate; PI(3)P, phosphatidylinositol 3-phosphate; PI(4)P, phosphatidylinositol 4-phosphate; PI(5)P, phosphatidylinositol 5-phosphate; PI(3,4)P_2, phosphatidylinositol 3,4-bisphosphate; PI(4,5)P_2, phosphatidylinositol 4,5-bisphosphate; PI(3,4,5)P_3, phosphatidylinositol 3,4,5-trisphosphate; RLD, regulator of chromosome condensation 1–like domain; UPS, ubiquitin-proteasome system; aa, amino acid; PDB, Protein Data Bank; HMW, high-molecular weight; IP, immunoprecipitation; ANOVA, analysis of variance.

Thus far, a total of 40 mutations in the *ALS2* gene has been reported in patients with MNDs (1, 2, 4, 5, 12–32). As most of them are frameshift or nonsense mutations, the resulting ALS2 variants either are unstable and thus liable to be degraded via the ubiquitin-proteasome system (UPS) (33) or are nonfunctional due to lack of the C-terminal Rab5 GEF domain (33). Recently, several missense or in-frame deletion mutations in the *ALS2* gene, which are predicted to code for mutant proteins preserving the C-terminal Rab5 GEF domain (*i.e.* $ALS2^{G49R}$ (13), $ALS2^{F65S}$ (12), $ALS2^{S100I}$ (14), $ALS2^{A120del}$ (15), $ALS2^{C157Y}$ (16), $ALS2^{P192L}$ (18), $ALS2^{G540E}$ (20), $ALS2^{A861\_T904del}$ (14), $ALS2^{S1116\_T1170del}$ (29), and $ALS2^{R1611W}$ (15)), were identified (Fig. S1). It has been reported that $ALS2^{C157Y}$ is preferentially degraded by the UPS when compared with WT ALS2 (16). In addition, we have demonstrated that, although both $ALS2^{C157Y}$ and $ALS2^{G540E}$ variants retain the Rab5 GEF activity *in vitro*, they fail to localize to macropinosomes and early endosomes upon Rac1 activation when ectopically expressed in cells (34). Thus, it is possible that such abnormal cellular behaviors of missense ALS2 variants are also implicated in loss of the ALS2 function. However, due to a limited number of pathogenic variants analyzed thus far, it is still too early to conclude as such, let alone underlying molecular mechanism for *ALS2*-linked MNDs.

Previously, we have shown that ALS2 interacts with itself through the C-terminal region, forming a homophilic oligomer (35). Importantly, this homo-oligomerization is not only crucial for the Rab5 GEF activity *in vitro* but also for the ALS2-mediated endosome fusion in cells (11, 35). These results lend credence to the hypothesis that structural abnormalities in pathogenic missense and/or in-frame deletion ALS2 variants are closely linked to loss of its cellular function, and therefore that formation of the proper ALS2 complex might be a prerequisite for Rac1-induced endosomal localization of ALS2 and the following activation of endosomal Rab5.

To prove this hypothesis, we here sought to clarify the relationship between intracellular localization and oligomeric states of several missense and in-frame deletion pathogenic ALS2 variants by conducting a series of immunocytochemical and biochemical analyses. In addition, to further gain insight into the structural basis of missense mutations, we generated a protein structure of N-terminal RLD harboring the majority of the missense pathogenic mutations, and we performed an *in silico* mutagenesis analyses to evaluate the potential effects of those mutations on the structure. We here demonstrated evidence showing that the altered oligomerization and/or destabilization of ALS2 was implicated in their impaired endosomal localization. Our data may provide important clues to understand the molecular mechanisms underlying the pathogenesis of *ALS2*-linked MNDs.

Results

Pathogenic ALS2 variants localize to Rac1-induced membrane ruffles but not to macropinosomes and early endosomes

Previously, we have demonstrated that the majority of the ectopically expressed WT ALS2 protein ($ALS2^{WT}$) is scattered throughout the cytoplasm in HeLa and COS-7 cells (10). Upon Rac1 activation, $ALS2^{WT}$ is recruited to membrane ruffles and then relocalized to macropinosomes and early endosomes via Rac1-stimulated macropinocytosis (11). By contrast, two pathogenic ALS2 variants, $ALS2^{C157Y}$ and $ALS2^{G540E}$, fail to be localized to macropinosomes and early endosomes (34).

To clarify the intracellular behavior of other missense as well as small in-frame deletion ALS2 variants, which have been newly identified but yet to be tested, we chose three representative pathogenic ALS2 variants: $ALS2^{S100I}$, the N-terminal RLD missense variant (14); $ALS2^{A861\_T904del}$, the central PH in-frame deletion variant (14); and $ALS2^{R1611W}$, the C-terminal VPS9 missense variant (15), in addition to $ALS2^{WT}$ and normal variant: $ALS2^{P132L}$. Using these variants, we investigated the changes in their intracellular distributions by the Rac1 activation. All variants were distributed throughout the cytoplasm in the absence of active Rac1 ($Rac1^{Q61L}$), similar to $ALS2^{WT}$ (Fig. 1*A*) and $ALS2^{P132L}$ (Fig. S2*A*). Upon Rac1 activation, $ALS2^{WT}$ was relocalized to the surface of large vesicular compartments, whereas the majority of variant proteins remained in the cytoplasm (Fig. 1*A*). Notably, despite that pathogenic ALS2 variants failed to localize to vesicular compartments, a significant portion of them was recruited to the Rac1-induced F-actin–positive membrane ruffles (Fig. 1*A*), reproducing the phenotypes of two previously examined ALS2 variants: $ALS2^{C157Y}$ and $ALS2^{G540E}$ (Fig. S2*B*).

Because the activation of Rac1 induced the formation of large vesicular compartments both in $ALS2^{WT}$ and ALS2 variant-overexpressing cells, we next investigated whether these vesicular compartments represented either macropinosomes or early endosomes and whether ALS2 was closely localized to these compartments. $ALS2^{WT}$ was not only present on the surface of the dextran-positive macropinosomes (Fig. 2*A*) but was also localized to EEA1-positive early endosomes (Fig. 1*B*). Line analysis clearly showed that the signals for engulfed dextran in macropinosomes were surrounded by those of $ALS2^{WT}$ (Fig. 2*B*). In contrast, all three pathogenic ALS variants examined, $ALS2^{S100I}$, $ALS2^{A861\_T904del}$, and $ALS2^{R1611W}$, were overlapped neither with dextran-positive macropinosomes nor with EEA1-positive endosomes (Figs. 1*B* and 2, *A* and *B*). Furthermore, coexpression of active Rac1 with $ALS2^{WT}$, but not with ALS2 variants, led to an enlargement of EEA1-positive endosomal compartments (Fig. 1*B*), consistent with our previous observations (34).

These results indicate that pathogenic ALS2 variants, which retain the C-terminal Rab5 GEF domain, lose their capability to internalize via Rac1-stimulated macropinocytosis. In other words, pathogenic ALS2 variants are defective in the localization to macropinosomes and/or early endosomes, even though they do not seem to hinder macropinocytosis itself and can be localized to membrane ruffles in cells.

Pathogenic ALS2 variants interact with themselves

We have previously reported that the ALS2 molecules self-interact through the N- and/or C-terminal regions (11, 35). It has also been shown that the pathogenic ALS2 variants, $ALS2^{C157Y}$ and $ALS2^{G540E}$, can interact with themselves (34). To confirm whether $ALS2^{S100I}$, $ALS2^{A861\_T904del}$, or $ALS2^{R1611W}$ self-interact, we conducted coimmunoprecipitation experi-

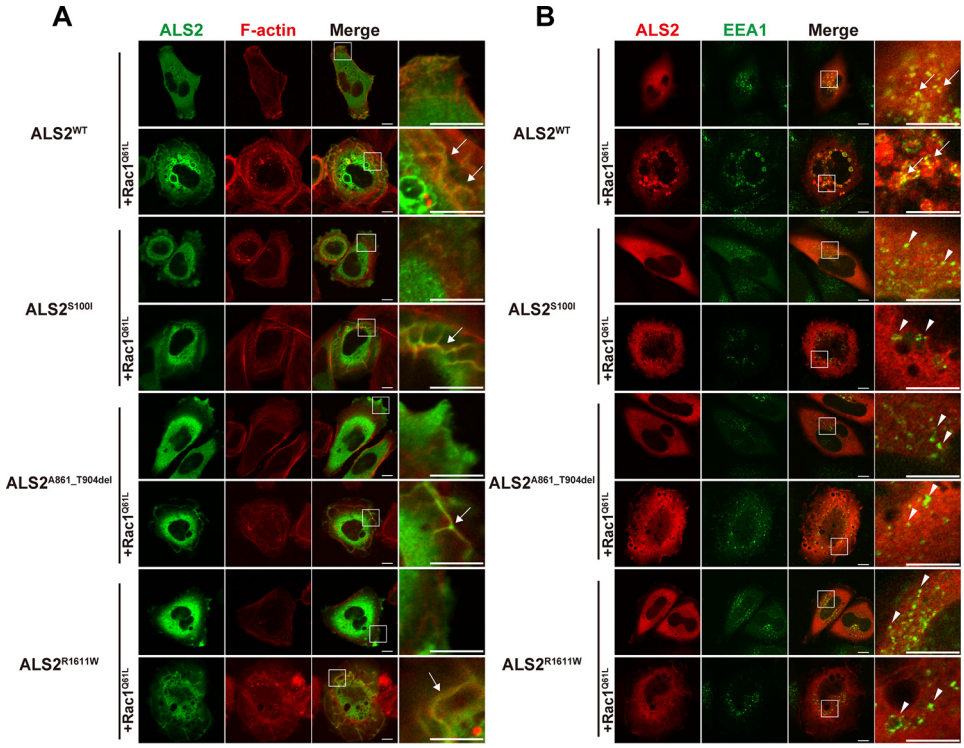

Figure 1. Pathogenic ALS2 variants localize to F-actin–positive dorsal ruffles or Rac1-induced membrane ruffles but not to EEA1-positive early endosomes. HeLa cells were transfected with pCIneoFLAG–ALS2^{WT}, pCIneoFLAG–ALS2^{S100I}, pCIneoFLAG–ALS2^{A861_T904del}, or pCIneoFLAG–ALS2^{R1611W} together with or without pCMV10–2xHA-Rac1^{Q61L} (*A* and *B*) or pCIneoFLAG-EEA1 (*B*). *A*, localization of ALS2 and its pathogenic variants to F-actin–positive membrane ruffles. The fixed cells were costained with anti-ALS2–RLD antibody (*green*) and Alexa 594-conjugated phalloidin (F-actin; *red*). *Arrows* indicate ALS2/phalloidin double-positive Rac1-induced membrane ruffles. *B*, redistribution of ALS2, but not the ALS2 variants, to early endosomal compartments. The fixed cells were costained with anti-ALS2–RLD (*red*) and anti-EEA1 (*green*) antibodies. *Arrows* and *arrowheads* indicate ALS2/EEA1 double-positive early endosomes and ALS2-negative EEA1-positive early endosomes, respectively. *A* and *B*, higher magnification images of the *boxed* regions are shown on the *right panels*. *Scale bars,* 10 μm.

ments. In all the cases examined; ALS2^{WT}, ALS2^{G540E}, ALS2^{S100I}, ALS2^{A861_T904del}, and ALS2^{R1611W}, the HA-tagged ALS2 molecules were efficiently coimmunoprecipitated with FLAG-tagged ones (Fig. 3). The results demonstrate that like ALS2^{WT}, missense or small in-frame deletion pathogenic ALS2 variants can interact with each other, indicating that pathogenic ALS2 variants could either homodimerize or homo-oligomerize in cells.

WT ALS2 forms a tetramer complex in mammalian cells

We have previously shown that both purified FLAG-tagged ALS2 and its artificial truncated mutant lacking both the N-terminal RLD and DH/PH domain of ALS2 (ALS2–MORN/VPS9) can form stable homophilic oligomers, presumably octamer, with no other detectable stable binding partners (36) and that this homo-oligomerization is crucial for the activation of Rab5 (35). Because the detergents used for the purification of the ALS2 proteins were different between the GEF assay, in which Tween 20 was used, and gel filtration, in which IGEPAL CA-630 was used, we tested the effects of differences in detergents as well as in the length of the storage period of purified ALS2 on the Rab5 GEF activity and oligomeric states. Surprisingly, we found that ALS2 in the solution containing Tween 20 kept stable activities for an approximate 1-year period when stored at 4 °C, whereas those in the solution containing IGEPAL CA-630 gradually lost their catalytic activity over a month with concomitant increase in sizes of the oligomeric complex (data not shown) (36). Thus, we suspected that an octameric form of the ALS2 complex *in vitro* (35) might not reflect the native form.

To determine the *bona fide* ALS2 complex in cells, we prepared fresh cell lysates from FLAG–ALS2^{WT}-expressing COS-7 cells without any purifications, used them for gel-filtration chromatography, and detected ALS2 by Western blotting using ALS2-specific antibody. As a result, ALS2^{WT} (~184 kDa) was eluted in fractions with an apparent peak molecular mass of ~700 kDa (Fig. 4, *A* and *B*). Importantly, this elution pattern was well matched to that of endogenous ALS2 in nontransfected cells (Fig. S3). Thus, it is reasonable that ALS2 forms a homophilic tetramer rather than an octamer in native conditions. Nonetheless, because the endogenous ALS2 complexes are slightly larger than those of overexpressed ALS2, it is still possible that the ALS2 complex contains some additional interactors *in vivo*.

To clarify how ALS2 formed a tetramer, we investigated the domain-mediated interactions of ALS2. As the ALS2 fragment lacking N-terminal RLD acts as a constitutive active form in cells (10), we first performed gel-filtration analysis of cell lysate prepared from FLAG–ALS2–DH/PH/MORN/VPS9 (~110 kDa) (Fig. S1)-expressing COS-7 cells. As a result, ALS2–DH/PH/MORN/VPS9 was eluted in fractions with a peak molecular mass of 400 – 600 kDa (Fig. S4), indicating that the majority of ALS2–DH/PH/MORN/VPS9 existed as a tetramer and/or

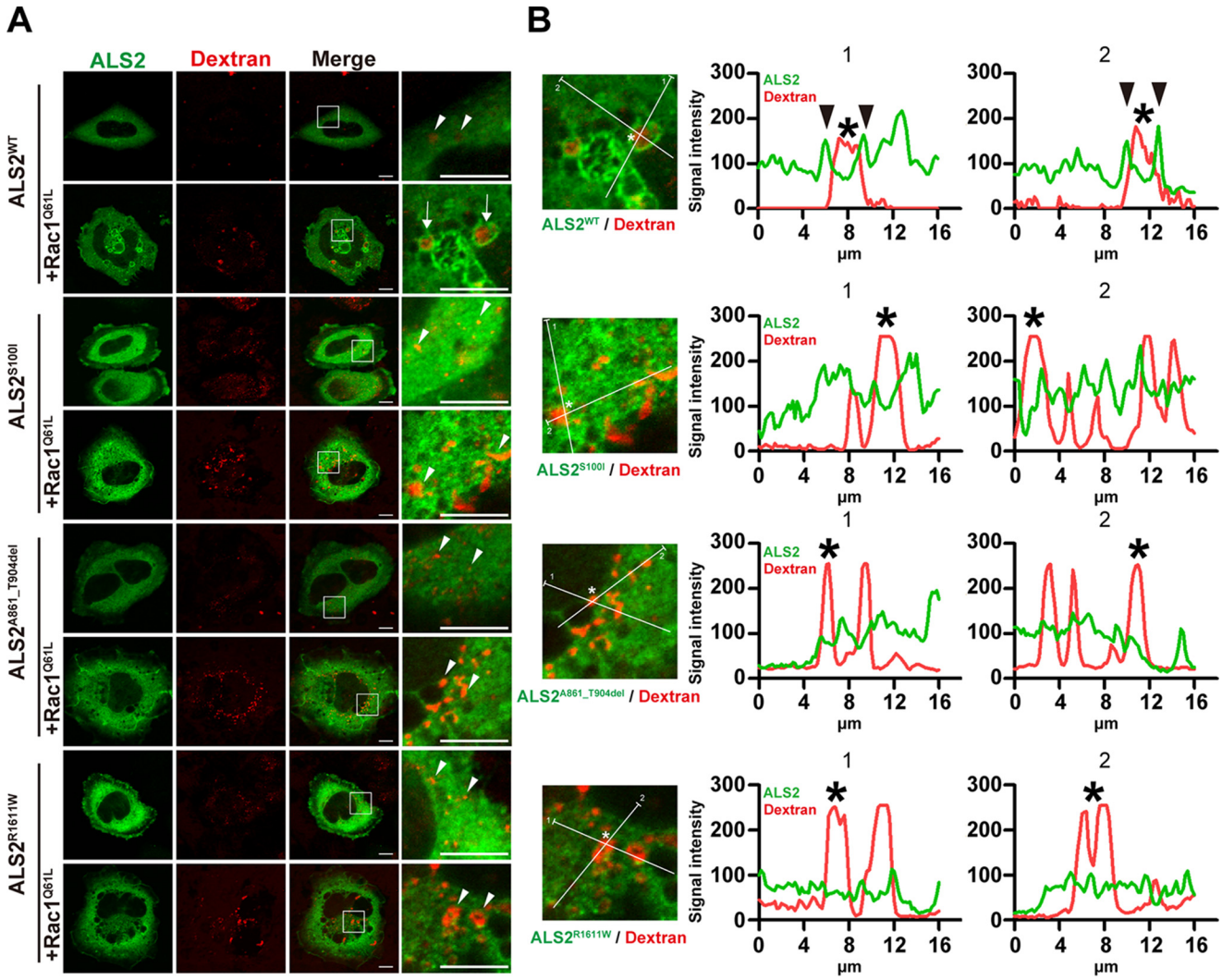

Figure 2. Pathogenic ALS2 variants do not redistribute to macropinosomes via Rac1-stimulated macropinocytosis. *A*, HeLa cells were transfected with pCIneoFLAG–ALS2^{WT}, pCIneoFLAG–ALS2^{S100I}, pCIneoFLAG–ALS2^{A861_T904del}, or pCIneoFLAG–ALS2^{R1611W} together with or without pCMV10–2xHA-Rac1^{Q61L}. The cells were treated with tetramethylrhodamine-conjugated dextran (70 kDa) (*red*). After fixation, the cells were stained with anti-ALS2–RLD antibody (*green*). Higher magnification images of the *boxed* regions are shown on the *right panels*. *Arrows* and *arrowheads* indicate ALS2-enwrapped dextran-positive and ALS2-negative dextran-positive macropinosomes, respectively. *Scale bars,* 10 μm. *B*, quantitative line analysis of the fluorescence intensities for ALS2 (*green*) and dextran (*red*) on dextran-positive macropinosomes. In each image, the *asterisk* indicates dextran-positive macropinosome of interest, and the end of the transverse *bar with the number* corresponds to the left end of the *x* axis of the graph. *Asterisks* and *arrowheads* noted in the graphs indicate the positions of dextran-positive macropinosome of interest and ALS2-localizing macropinosomal membranes, respectively.

larger complex. Because the C-terminal region of ALS2 between MORN and VPS9, which covered the Rab5 GEF catalytic domain (10, 35), directly mediated self-interaction (35), we next conducted gel-filtration analysis of cell lysate prepared from FLAG–ALS2–MORN/VPS9-expressing (Fig. S1) COS-7 cells as well as the recombinant purified ALS2–MORN/VPS9 protein prepared from bacterial cultures. Both FLAG–ALS2–MORN/VPS9 and the recombinantly purified ALS2–MORN/VPS9 (molecular mass was ~70 kDa for each) were eluted in fractions with an apparent peak molecular mass of ~160 kDa (Fig. S5), indicative of a dimeric complex of the C-terminal MORN/VPS9 region of ALS2.

Taken together, it is predicted that the dimeric ALS2 complex, which interacts through the C-terminal MORN/VPS9 region in an antiparallel fashion (35), can further interact with each other in a DH/PH domain-dependent manner, forming a tetrameric ALS2 complex in cells. It is also suggested that the RLD of ALS2 is not essential to form a proper tetrameric complex, even though it retains the ability to interact with the C-terminal region of ALS2 (11).

Pathogenic ALS2 mutations alter the oligomeric states of the ALS2 complex

To define the oligomeric states of normal ALS2 variants (ALS2^{P132L} and ALS2^{E1173K}; rs# cluster ID/NCBI Assay IDs rs41308810/ss65624394 and rs41309046/ss65624421, respectively) (dbSNP, LOCUSID 57679), Rab5 GEF-defective artificial mutant (ALS2^{P1603A}), and Rab5 GEF-defective/endosomal localization-defective artificial mutant (ALS2^{L1617A}) (10), we performed gel-filtration analysis under the same experimental conditions. As a result, the elution patterns for ALS2^{P132L}, ALS2^{E1173K}, and ALS2^{P1603A} were mostly similar to those of ALS2^{WT}, except there was a minor peak at an apparent molecular mass of ~1000 kDa in these variants or mutants (Fig. 4, *A*

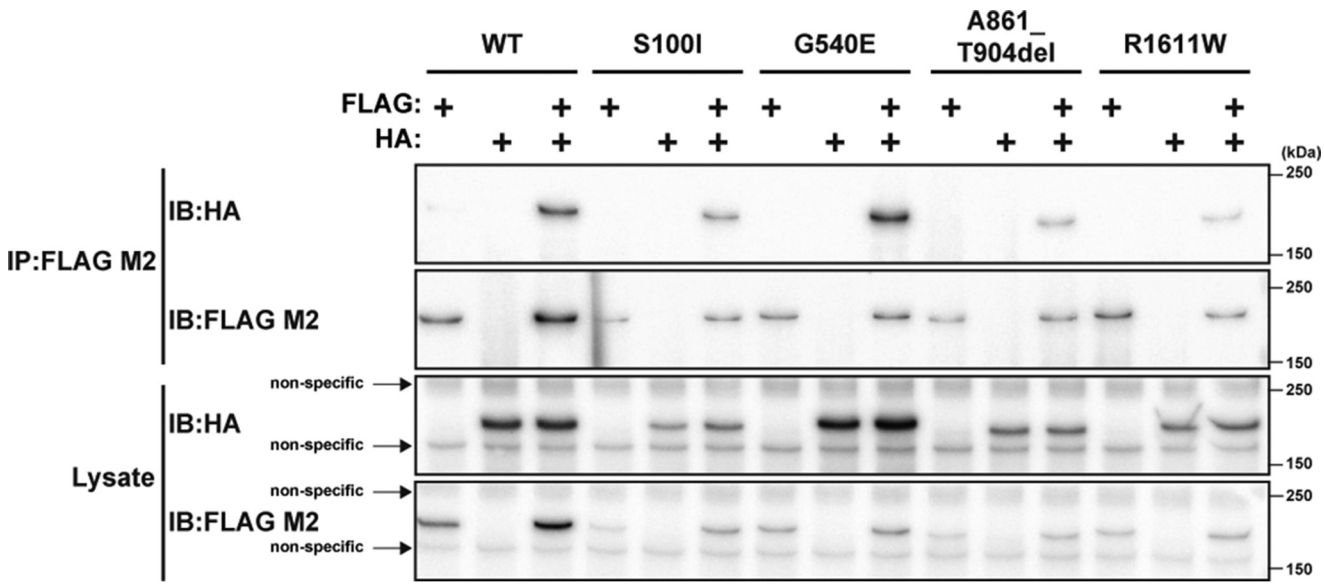

Figure 3. Pathogenic ALS2 variants interact with themselves. COS-7 cells were transfected with single expression construct, including pCIneoFLAG–ALS2^{WT}, pCIneoHA-ALS2^{WT}, pCIneoFLAG–ALS2^{S100I}, pCIneoHA-ALS2^{S100I}, pCIneoFLAG–ALS2^{G540E}, pCIneoHA-ALS2^{G540E}, pCIneoFLAG–ALS2^{A861_T904del}, pCIneoHA-ALS2^{A861_T904del}, pCIneoFLAG–ALS2^{R1611W}, and pCIneoHA-ALS2^{R1611W}, or were double-transfected with pairs of FLAG- and HA-tagged ALS2 expression constructs as indicated. Cell lysates were subjected to immunoprecipitation with anti-FLAG M2 antibody. Both cell lysates and immunoprecipitates were analyzed by Western blotting using antibodies as indicated; *IP,* antibody used for immunoprecipitation; *IB,* antibody used for Western blot analysis.

and *B*). Interestingly, the elution pattern for ALS2^{L1617A} was different from others, in which ALS2^{L1617A} was eluted in a wide range of fractions with dual major peaks (~400 and ~700 kDa) and a single minor peak (~1000 kDa) (Fig. 4, *A* and *B*).

Next, we investigated the oligomeric states for the missense and small in-frame deletion pathogenic ALS2 variants (ALS2^{G49R}, ALS2^{S100I}, ALS2^{C157Y}, ALS2^{G540E}, ALS2^{A861_T904del}, and ALS2^{R1611W}). Unlike ALS2^{WT}, the distributions of all pathogenic variants except for ALS2^{R1611W} were shifted toward the high-molecular weight fractions with two apparent peaks of ~700 and ~1000 kDa (Fig. 4, *C* and *D*). In contrast, ALS2^{R1611W} was broadly eluted in fractions with apparent molecular masses ranging from ~400 to ~700 kDa and an additional single minor peak of ~1000 kDa (Fig. 4, *C* and *D*), which was similar to those of ALS2^{L1617A} mutant.

These results demonstrate that nonpathogenic ALS2 variants (ALS2^{P132L} and ALS2^{E1173K}) as well as the Rab5 GEF-defective artificial mutant (ALS2^{P1603A}) primarily exist as tetrameric forms like ALS2^{WT}. However, ALS2 carrying missense pathogenic mutations in the N-terminal RLD (ALS2^{G49R}, ALS2^{S100I}, ALS2^{C157Y}, and ALS2^{G540E}) or in-frame deletion in the central PH domain (ALS2^{A861_T904del}) exist as abnormally higher molecular weight complexes. By contrast, both Rab5 GEF-defective/endosomal localization-defective artificial mutant (ALS2^{L1617A}) and the C-terminal VPS9 missense pathogenic variant (ALS2^{R1611W}) exist as dimeric and/or trimeric smaller forms. Thus, pathogenic mutations lead to structural distortion of the ALS2 oligomeric complexes.

ALS2–RLD^{WT} and mutant RLDs were localized to phalloidin-positive F-actin

We have previously demonstrated that the ectopically-expressed ALS2–DH/PH/MORN/VPS9 fragment lacking the N-terminal RLD is instantly localized to early endosomes and induces their enlargements (10). In addition, the activation of Rac1 results in relocalization of full-length ALS2 from the cytoplasm to membrane ruffles and then to macropinosomes and/or early endosomes via macropinocytosis and heterotypic vesicle fusions (11). Thus, we consider that although the RLD of ALS2 acts as a suppressor for the recruitment of ALS2 to membranous compartments in a dormant state (10), it may rather function as a recruiter of ALS2 to membrane ruffles upon Rac1 activation. Taking into account the fact that 7 of 10 missense or in-frame deletion mutations that have been reported thus far are densely localized to the N-terminal RLD of ALS2, the RLD might have crucial roles in the intracellular behavior of ALS2.

To clarify the molecular tropism and function of the RLD, we investigated the localization of the RLD fragment of ALS2 (ALS2–RLD) in cells. Although all the mutants examined, ALS2–RLD^{S100I}, ALS2–RLD^{C157Y}, and ALS2–RLD^{G540E}, were primarily distributed throughout the cytoplasm, a portion of them were colocalized with phalloidin-positive F-actin on membrane ruffles under Rac1-activating conditions, as were ALS2–RLD^{WT} and ALS2–RLD^{P132L} (Fig. 5, *A* and *B*). It was also noted that all the missense pathogenic ALS2 mutants could be recruited to membrane ruffles but failed to be relocalized to macropinosomes and/or early endosomes by the Rac1 activation (Figs. 1 and 2). The results combined suggest that the RLD carrying missense pathogenic mutations still retains the ability to mediate the localization of ALS2 to membrane ruffles but not to macropinosomes and/or endosomes.

ALS2–RLD^{WT} and mutant RLDs have similar affinity profiles toward phosphatidylinositols

Several phosphatidylinositol molecules play an important role in the spatiotemporal regulation of membrane-associated proteins in macropinocytosis as well as in vesicle trafficking and

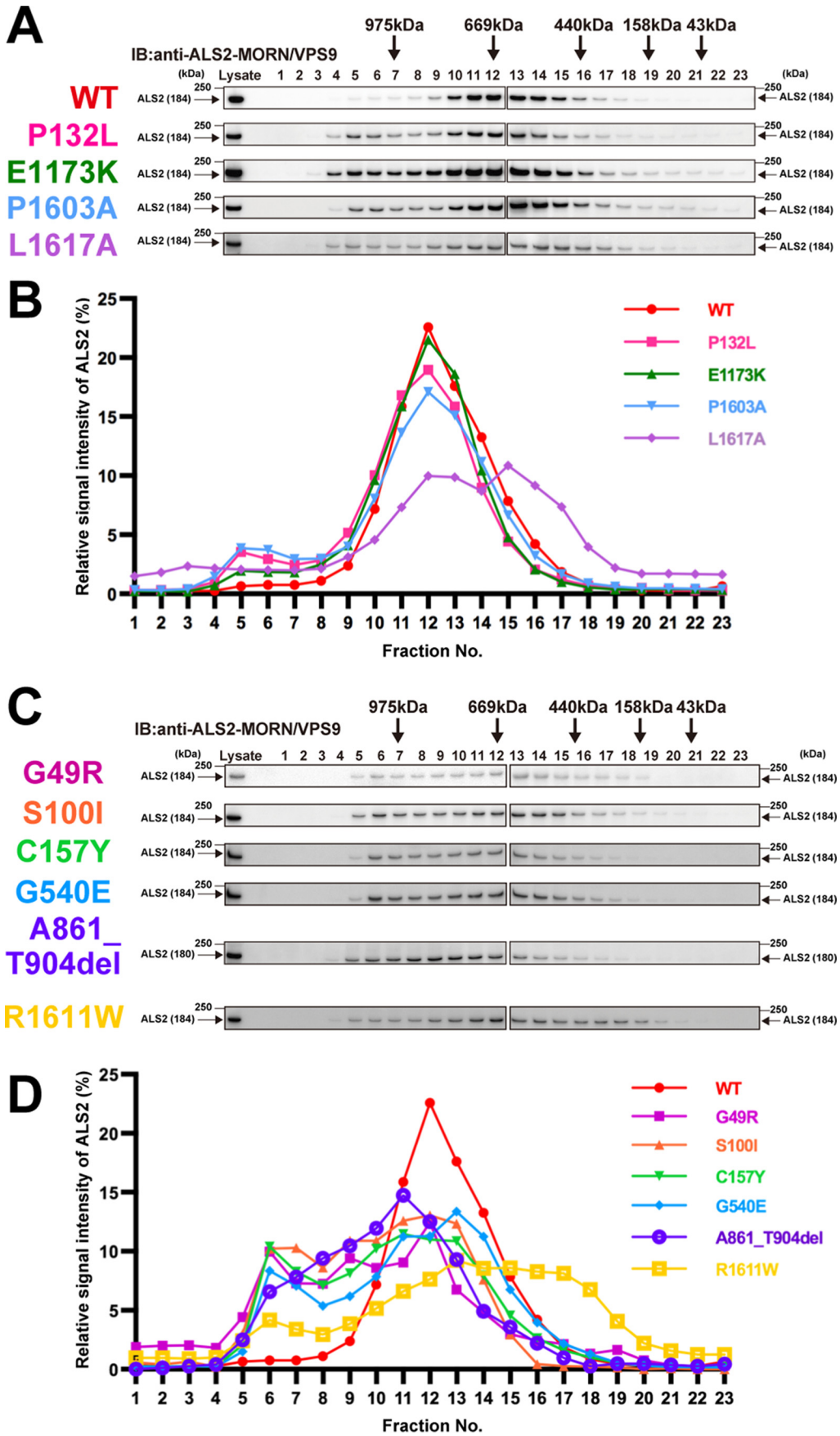
A
975kDa
669kDa
440kDa
158kDa
43kDa
IB:anti-ALS2-MORN/VPS9
(kDa)
Lysate
1 2 3 4 5 6 7 8 9 10 11 12 13 14 15 16 17 18 19 20 21 22 23
WT
P132L
E1173K
P1603A
L1617A
ALS2 (184)
250
B
Relative signal intensity of ALS2 (%)
Fraction No.
WT
P132L
E1173K
P1603A
L1617A
C
G49R
S100I
C157Y
G540E
A861_
T904del
R1611W
ALS2 (180)
D
WT
G49R
S100I
C157Y
G540E
A861_T904del
R1611W

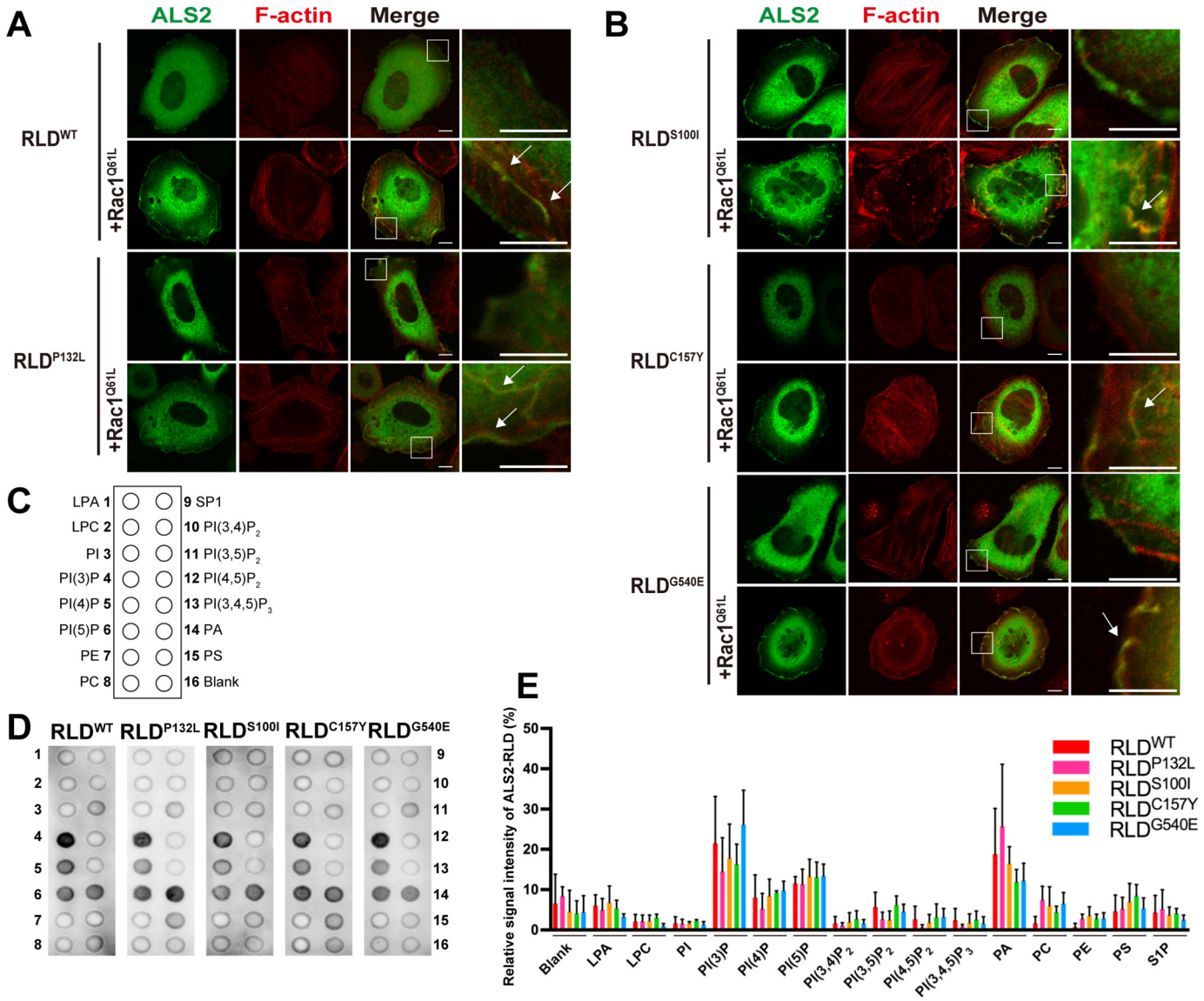

Figure 5. Intracellular localization and the affinity profiles toward phosphatidylinositols of the ALS2–RLD fragment carrying pathogenic mutations. *A* and *B*, localization of ALS2–RLD and its pathogenic mutants to F-actin–positive membrane ruffles. HeLa cells were transfected with pCIneoFLAG–ALS2–RLD^{WT}, pCIneoFLAG–ALS2–RLD^{P132L}, pCIneoFLAG–ALS2–RLD^{S100I}, pCIneoFLAG–ALS2–RLD^{C157Y}, or pCIneoFLAG–ALS2–RLD^{G540E} together with or without pCMV10–2xHA-Rac1^{Q61L}. The fixed cells were costained with anti-ALS2–RLD antibody (*green*) and Alexa 594-conjugated phalloidin (F-actin; *red*). *Arrows* indicate ALS2/F-actin double-positive Rac1-induced membrane ruffles. *Scale bars,* 10 μm. *C*, layout of PIP strip. *Spot 1*, lysophosphatidic acid (*LPA*); *spot 2,* lysophosphocholine (*LPC*); *spot 3,* phosphatidylinositol (*PI*); *spot 4,* PI(3)P; *spot 5,* PI(4)P; *spot 6,* PI(5)P; *spot 7,* phosphatidylethanolamine (*PE*); *spot 8,* phosphatidylcholine (*PC*); *spot 9,* sphingosine 1-phosphate (*S1P*); *spot 10,* PI(3,4)P_2; *spot 11,* PI(3,5)P_2; *spot 12,* PI(4,5)P_2; *spot 13,* PI(3,4,5)P_3; *spot 14,* phosphatidic acid (*PA*); *spot 15,* phosphatidylserine (*PS*); *spot 16, Blank*. *D*, lipid overlay assay for the ALS2–RLD fragment. ALS2–RLD^{WT}, ALS2–RLD^{S100I}, ALS2–RLD^{P132L}, ALS2–RLD^{C157Y}, and ALS2–RLD^{G540E} were incubated with PIP Strips^{TM}, and bound ALS2 molecules were detected by ALS2–RLD antibody. *E*, quantitative analysis of signal intensities of ALS2 molecules. Each value is expressed as a mean (± S.D.) percentage of the total signal intensity representing ALS2 on each strip ($n = 4$). Statistical significance was evaluated by one-way ANOVA with Bonferroni's multiple comparison test.

fusion (37). We have previously demonstrated that two missense pathogenic ALS2 variants, ALS2^{C157Y} and ALS2^{G540E}, show a lower affinity to specific phosphoinositide phosphates (PIPs), particularly to PI(3)P, PI(4,5)P_2, and PI(3,4,5)P_2 (34), suggestive of the regulatory mechanism for macropinosomal localization of ALS2. To clarify the affinities of ALS2–RLD

Figure 4. Gel-filtration analysis of WT ALS2 and its variants. *A*, Western blot analysis of the gel-fractionated FLAG-tagged ALS2 and its variants and/or mutants. Lysates from COS-7 cells that were transfected with pCIneoFLAG–ALS2^{WT}, pCIneoFLAG–ALS2^{P132L}, pCIneoFLAG–ALS2^{E1173K}, pCIneoFLAG–ALS2^{P1603A}, or pCIneoFLAG–ALS2^{L1617A} and were applied to the Superose6 10/300 gel-filtration column. Cell lysates and the fractions were analyzed by Western blotting using anti-ALS2–MORN/VPS9 antibody. *Arrows* indicate the positions of molecular mass markers. *B*, quantitative analysis of signal intensities of ALS2 molecules. Each fraction was expressed as a mean percentage of the total amount of signals representing ALS2 across the entire fractions ($n = 4$). *C*, Western blot analysis of the gel-fractionated FLAG-tagged pathogenic ALS2 variants. Lysates from COS-7 cells that were transfected with pCIneoFLAG–ALS2^{G49R}, pCIneoFLAG–ALS2^{S100I}, pCIneoFLAG–ALS2^{C157Y}, pCIneoFLAG–ALS2^{G540E}, pCIneoFLAG–ALS2^{A861_T904del}, or pCIneoFLAG–ALS2^{R1611W} and were applied to the Superose6 10/300 gel-filtration column. Cell lysates and the fractions were analyzed as shown in *A*. *Arrows* indicate the positions of molecular mass markers. *D*, quantitative analysis of signal intensities of ALS2 molecules. Each fraction is expressed as a mean percentage of the total signal intensity representing ALS2 across the entire fractions ($n = 4$; except for G49R mutant ($n = 1$)). For comparison, data for ALS2^{WT} that are the same as those shown in *B* are included.

toward PIP molecules, we performed protein–lipid overlay assay using the ALS2–RLD fragments as probes. All the ALS–RLD peptides, ALS2–RLD^{WT}, normal variant ALS2–RLD^{P132L}, and pathogenic missense ALS2–RLD mutants, bound to specific PIPs with different degrees of affinity (Fig. 5, *D* and *E*). However, unlike the cases of full-length ALS2 (34), the differences in the patterns of lipid affinity between WT and mutated RLD were not statistically significant (Fig. 5, *D* and *E*). The results indicate that missense mutations themselves, at least in the N-terminal RLD, do not alter their affinity toward PIPs, consistent with the unaltered intercellular distribution of ALS2–RLD mutants observed (Fig. 5, *A* and *B*).

ALS2–RLD^{WT} can form multiple types of high-molecular weight protein complexes

We have previously reported that the N-terminal RLD can interact with the C-terminal MORN/VPS9 region of ALS2 (11). Furthermore, coimmunoprecipitation experiments demonstrated that the RLD self-interacted (data not shown). However, the oligomeric structure of the RLD complex is still undetermined. To address this issue, we conducted gel-filtration analysis of fresh cell lysates prepared from FLAG–ALS2–RLD^{WT}-expressing COS-7 cells and the recombinant-purified ALS2–RLD^{WT} prepared from bacterial cultures. FLAG–ALS2–RLD^{WT} (~73 kDa) was eluted in a wide range of fractions with three apparent peaks of ~150, ~700, and ~1000 kDa with the highest at ~150 kDa (Fig. 6, *A* and *B*). Interestingly, purified ALS2–RLD^{WT} was eluted in fractions with two apparent peaks ranging from 400 to 700 and ~1000 kDa with no observable signals representing low-molecular mass complexes (Fig. S6). Thus, it is likely that ALS2–RLD^{WT} can exist as a dimeric form in cells, but it easily forms multiple high-molecular mass complexes, probably tetramer to octamer (400–700 kDa) or much larger complexes (~1000 kDa) of ALS2–RLD *in vitro*, suggesting that the ALS2–RLD fragment may be intrinsically aggregation-prone.

Some pathogenic mutations in the RLD alter the oligomeric states of the ALS2–RLD fragment

Next, we investigated the oligomeric states of ALS2–RLD carrying normal variation ALS–RLD^{P132L} or missense pathogenic mutations ALS2–RLD^{S100I}, ALS2–RLD^{C157Y}, and ALS2–RLD^{G540E}. Signal distributions for some of these mutants were slightly shifted toward high-molecular weight fractions with concomitant decrease in the signal intensity of ~150 kDa dimeric fractions (Fig. 6, *A* and *B*). Indeed, quantitative analysis revealed that although the total signal intensities in high-molecular weight (HMW) fractions (fractions 1–8) for these mutants were comparable with that for ALS2–RLD^{WT}, tetra-octameric fractions (fractions 9–16) for ALS2–RLD^{S100I}, ALS2–RLD^{P132L}, and ALS2–RLD^{C157Y} were significantly higher than that for ALS2–RLD^{WT} with a concomitant decrease in their dimeric fractions (fractions 17–23) (Fig. 6*C*). These data indicate that some pathogenic missense mutations as well as normal variation in the N-terminal RLD can alter the oligomeric states of the ALS2–RLD fragment.

RLD of ALS2 is predicted to form a seven-bladed β-propeller

To clarify the structural and functional implications of missense mutations in the RLD of ALS2, we adopted the optimal target-template alignment approach and built a structural model for the ALS2–RLD fragment. First, we performed a BLASTP search against the PBD database using ALS2–RLD sequence as a query. The third RLD of human HERC2 (PDB code 3KCI) was selected as a template. Alignment of amino acid sequences between target (ALS2–RLD) and template (PDB code 3KCI) revealed that the N-terminal RLD of ALS2 encoded a seven-bladed β-propeller (Figs. 7 and 8 and Fig. S7). It was noted that among seven blades, two were predicted to be discontinuous, in which blade five was interrupted by 306 aa of intercalated disordered sequence (residues 219–524) (Figs. 7 and 8), and blade 1 consisted of two separate sequences; both ends correspond to N- and C-terminal regions of the RLD (residues 1–39 and 664–690, respectively) (Fig. 7). The three-dimensional ribbon representation of the RLD structure model in conjunction with the surface property prediction revealed that the "top face" of the propeller showed a hydrophilic nature, whereas the "bottom face" with an open central hole formed a hydrophobic cluster (Fig. 8, *A* and *B*, and Fig. S8), suggesting that the bottom face is implicated in the protein interactions. These results are fully consistent with the previously reported model, which was built based upon the human RCC1 sequence as a template (62).

Pathogenic mutations in the RLD reduce protein stability

To predict the effects of mutations and/or variations in the structure of the RLD, the position of the residues for six pathogenic missense mutations (Gly-49, Phe-65, Ser-100, Cys-157, Pro-192, and Gly-540), a single-residue deletion (Ala-120), and a variant in healthy individuals (Pro-132) was plotted on the three-dimensional ribbon representation of the RLD structure model (Fig. 8*A*). All residues except for Pro-192 were predicted to be exposed to the protein surface close to the top face of blades 2–5 (Fig. 8*A*). It is also noted that all mutations are localized within the seven-bladed propeller and not to the intercalated disordered sequence, suggesting that the structural distortion in the propeller is implicated in dysfunctional RLD of ALS2.

Next, to evaluate the effect of each mutation on the protein stability, we performed molecular dynamics simulations using CHARMm force field and calculated the difference in the folding free energy of the mutant and WT structures. The simulations showed that all pathogenic mutations but P192L reduced the protein stability (mutation energy >0.5 kcal/mol) (Table 1). In particular, the S100I, C157Y, and G540E mutations strongly affected the protein stability (15.90, 4.49, and 10.09 kcal/mol, respectively). In contrast, the values of the mutation energy for P132L and P192L were 0.52 and 0.41 kcal/mol, respectively, both of which were lower than or very close to the cutoff value (0.5 kcal/mol), indicating that the protein structure is minimally affected by these variations. It is noted that homozygous P192L mutation was originally identified in Japanese patients with sporadic juvenile ALS (18) and that pathogenicity of the P192L mutation has yet to be validated. Therefore, it is still

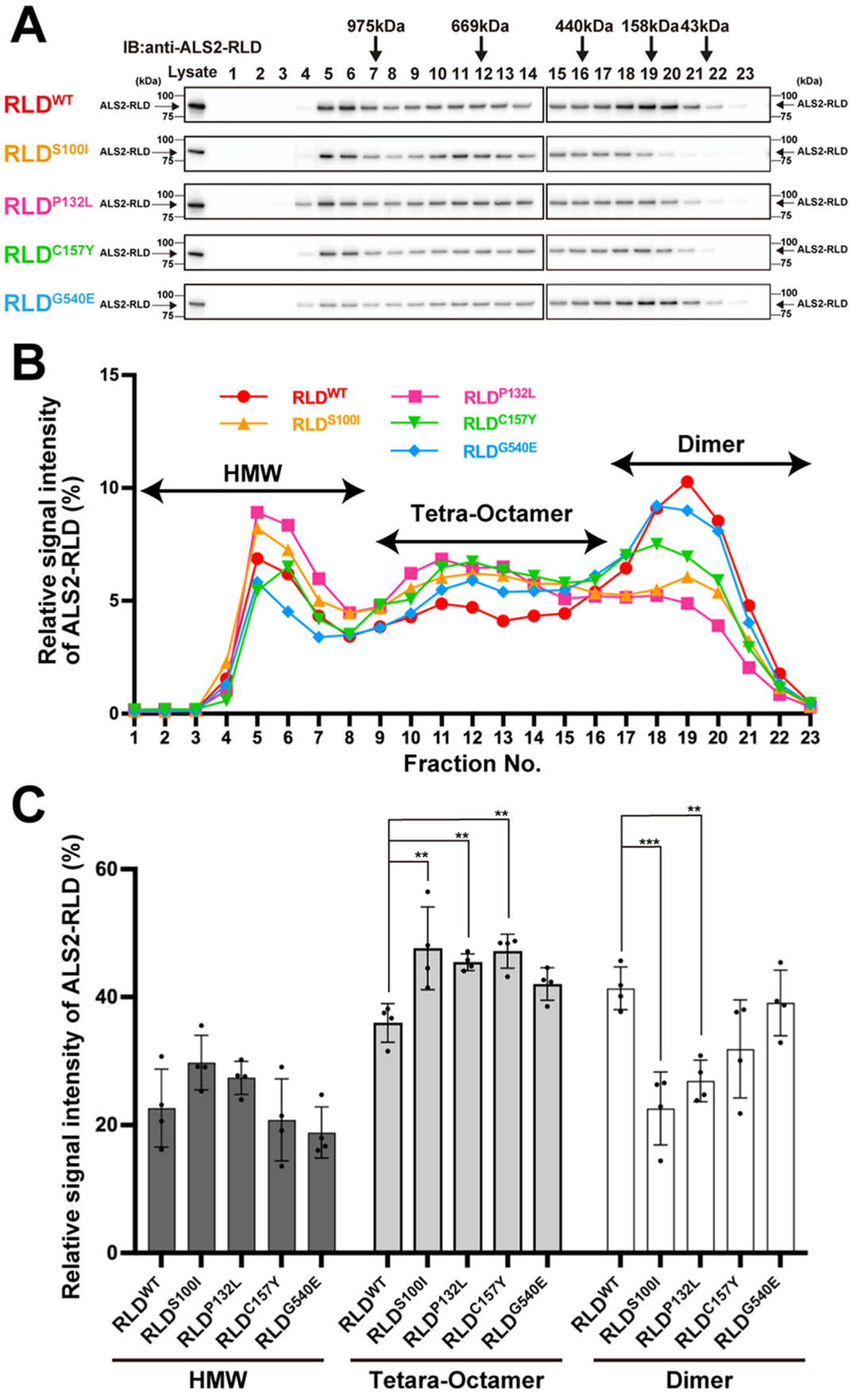
A
IB:anti-ALS2-RLD
975kDa
669kDa
440kDa
158kDa
43kDa
Lysate 1 2 3 4 5 6 7 8 9 10 11 12 13 14 15 16 17 18 19 20 21 22 23
(kDa)
RLDWT
RLDS100I
RLDP132L
RLDC157Y
RLDG540E
ALS2-RLD
100
75
B
Relative signal intensity of ALS2-RLD (%)
HMW
Tetra-Octamer
Dimer
Fraction No.
C
Relative signal intensity of ALS2-RLD (%)
HMW
Tetara-Octamer
Dimer

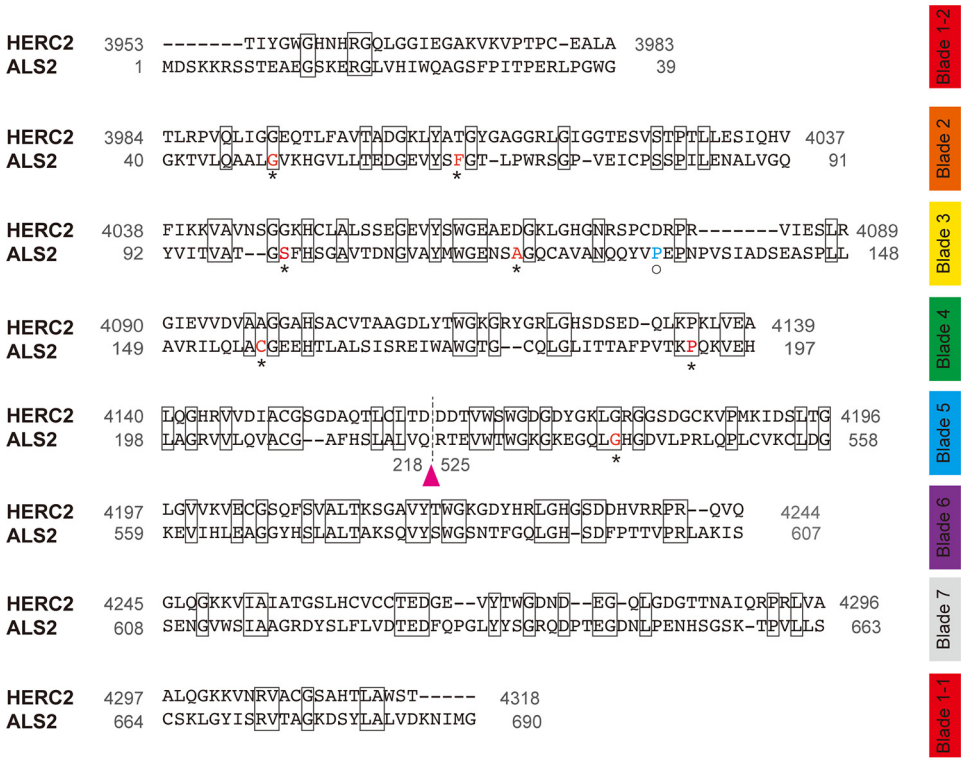

Figure 7. Amino acid sequence alignment corresponding to the region of seven-bladed β-propeller for ALS2–RLD and HERC2-RLD3 (PDB code 3KCI). Identical residues are *boxed*. *Asterisks* and *open circle* indicate residues of pathogenic ALS2 mutations and of normal ALS2 variations, respectively. *Magenta arrowhead* indicates the position at which 306 aa of the disordered sequence spanning 218–525 aa for ALS2–RLD are inserted.

possible that like P132L, P192L merely represents a rare normal variant of ALS2.

As the residues at positions 100, 132, 157, and 540 were exposed to the protein surface, we further assessed the surface hydrophobicity. However, there were no significant differences in the hydrophobicity around these four residues between variants and WT (Fig. S9), indicating that the local surface hydrophobicity might not be responsible for the functional alteration in the pathogenic ALS2 variants. Taken together, the results imply that missense pathogenic mutations in the RLD of ALS2 destabilize the normal protein structure, namely the architecture for seven-bladed β-propeller.

Some pathogenic mutations decrease the stability of the full-length ALS2 protein in NSC-34 cells

It has previously been shown that pathogenic frameshift ALS2 mutants and ALS2^{C157Y} were both unstable and thus rapidly degraded in cells (16, 33). To examine whether other pathogenic missense mutations as well as normal variation affected the stability in ALS2, we performed the cycloheximide (CHX) chase assay using the NSC-34 motor neuron-like hybrid cell line (Fig. 9, *A* and *B*). The levels of ALS2 in all constructs examined were significantly decreased by 8 h after the CHX treatment (Table S1). For the normal ALS2 variant, ALS2^{P132L} showed comparable stability with ALS2^{WT}. By contrast, 4 h after the CHX treatment, the levels of all pathogenic variants, ALS2^{S100I}, ALS2^{C157Y}, and ALS2^{G540E}, except for ALS2^{G49R}, were significantly lower than that of ALS2^{WT} (Fig. 9*B*), indicating that some, but not all, pathogenic variants were unstable and thus degraded faster than ALS2^{WT}. It was remarkable that these *in vitro* results were consistent with those for *in silico* predictions, in which three mutations, S100I, C157Y, and G540E, exhibited higher mutation energy among others (Table 1).

Discussion

Previously, it has been shown that ALS2 forms a homophilic oligomer and acts as a GEF for Rab5 (35). This oligomerization is crucial not only for the Rab5 activation *in vitro* but also for the ALS2-mediated endosome fusion and maturation in cells (11, 35). Recently, we have shown that pathogenic missense ALS2 variants, which retain the Rab5 GEF activity, fail to properly localize to endosomes via Rac1-stimulated macropinocytosis (34). However, molecular mechanisms underlying dysregulated

Figure 6. Gel-filtration analysis of the WT ALS2–RLD and those carrying pathogenic mutations. *A*, Western blot analysis of the gel-fractionated FLAG-tagged ALS2–RLD and its pathogenic mutants. Lysates from COS-7 cells that were transfected with pCIneoFLAG–ALS2–RLD^{WT}, pCIneoFLAG–ALS2^{P132L}, pCIneoFLAG–ALS2–RLD^{S100I}, pCIneoFLAG–ALS2–RLD^{C157Y}, or pCIneoFLAG–ALS2–RLD^{G540E} and were applied to the Superose6 10/300 gel-filtration column. Cell lysates and the fractions were analyzed by Western blotting using anti-ALS2–RLD antibody. *Arrows* indicate the positions of molecular mass markers. *B*, quantitative analysis of signal intensities of ALS2 molecules. Each fraction is expressed as a mean percentage of the total signal intensity representing ALS2 across the entire fractions ($n = 4$). *C*, relative abundance of HMW, tetra-octameric, and dimeric ALS2–RLD complex. Values of the HMW (*fraction 1–8*), tetra-octameric form (*fraction no. 9–16*), and dimeric form (*fraction no. 17–23*) are expressed as mean (± S.D.) percentages of the total signal intensity representing ALS2–RLD ($n = 4$). Individual data points are also shown. Statistical significance was evaluated by one-way ANOVA with Bonferroni's multiple comparison test (**, $p < 0.01$; ***, $p < 0.001$).

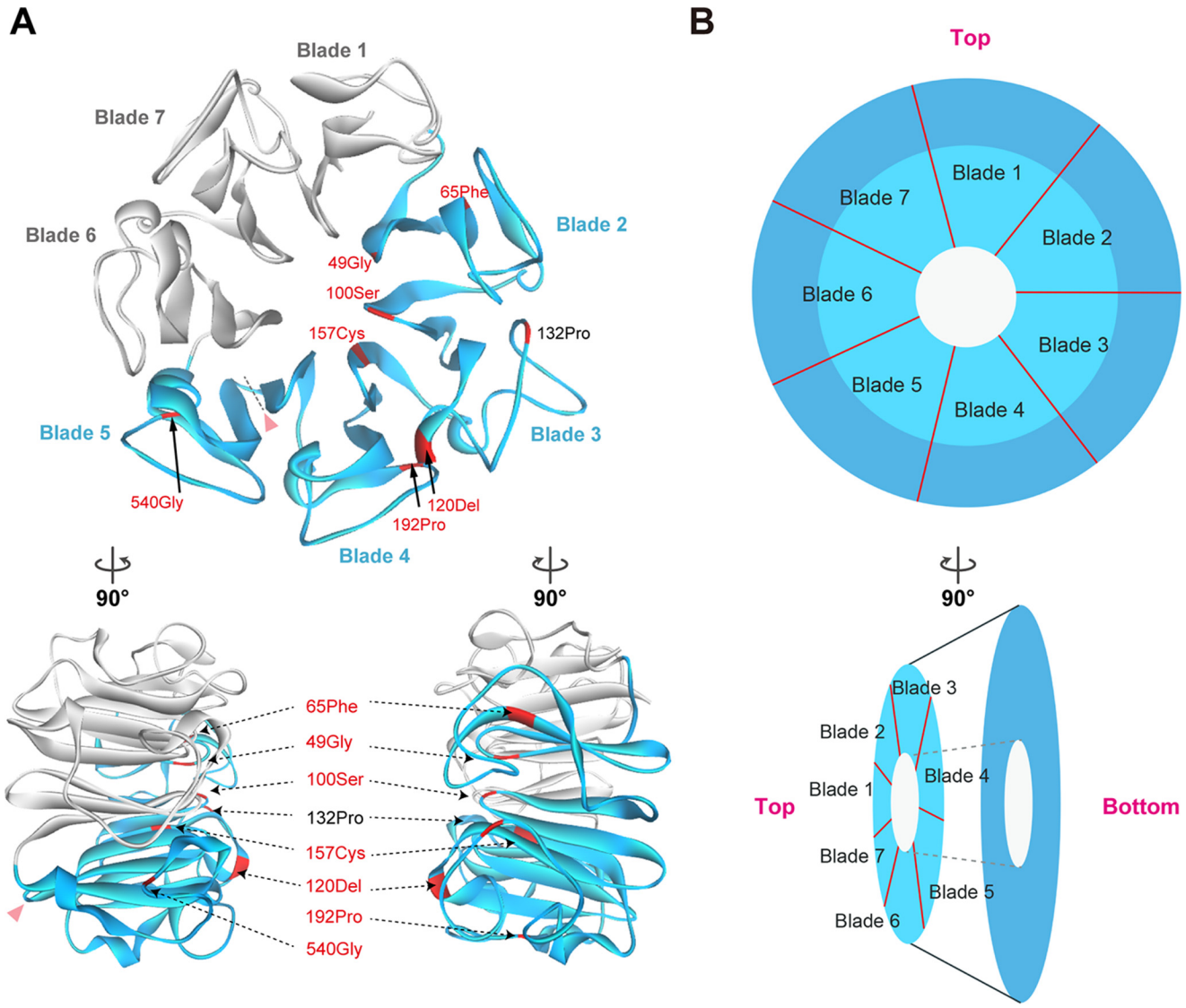

Figure 8. Homology model of the β-propeller of ALS2–RLD. *A,* three-dimensional ribbon representation of the seven-bladed β-propeller structure model for ALS2–RLD. The positions of residues corresponding to seven pathogenic mutations and single normal variation are marked in *red color*. It is noted that all the mutations/variations reside within blades 2–5 (shown in "*blue*" ribbons). *Top panel,* axial view along the central shaft of the propeller structure. *Bottom panels,* protein structure on the *top panel* is rotated by ±90° about the *y* axis. *Magenta arrowhead* indicates the position at which the disordered sequence is inserted in ALS2–RLD. *B, cartoon* diagrams for top and bottom of the seven-bladed β-propeller structure model for ALS2–RLD. *Top panel,* axial view from the top side of the propeller structure. *Bottom panel,* protein structure on the *top panel* is rotated by 90° about the *y* axis.

Table 1

Protein stability for the wildtype and mutated RLDs of ALS2

When the values of difference in the free energy between the mutated and wildtype structures are >0.5, they are defined as "destabilizing."

Residue	Mutation	Mutation energy	Effect of mutation
49	Gly to Arg	1.06	Destabilizing
65	Phe to Ser	1.03	Destabilizing
100	Ser to Ile	15.9	Destabilizing
132	Pro to Leu	0.52	Neutral
157	Cys to Tyr	4.49	Destabilizing
192	Pro to Leu	0.41	Neutral
540	Gly to Glu	10.09	Destabilizing

distribution of ALS2 variants are still unclear. To address this issue, we sought to clarify the relationship between intracellular localization and oligomeric states of several missense and in-frame deletion pathogenic ALS2 variants. Here, we demonstrated evidence showing that ALS2 formed a homophilic tetramer in native conditions, and pathogenic mutations might destabilize the protein structure thereby altering the oligomeric states and intracellular behavior of ALS2.

It has been widely accepted that complex formation is one of the fundamentally important molecular features for GEFs in their catalytic exchanging reaction of GDP for GTP on-target small GTPases in response to upstream signals. Among the VPS9 domain-containing Rab5 GEFs, RABGEF1/Rabex-5, one of the well characterized Rab5 GEFs, has been shown to form a heteromeric complex with Rabaptin-5, thereby enhancing the RABGEF1-mediated Rab5 GEF activity and facilitating endosome fusions (38). However, RIN2 (Rab interactor 2), a member of the VPS9 domain containing RIN family proteins, is known to form a homophilic tetramer through the interaction of two anti-parallel RIN2 dimers to each other (39, 40). It has also been reported that the activation of small GTPase Rab7 is mediated

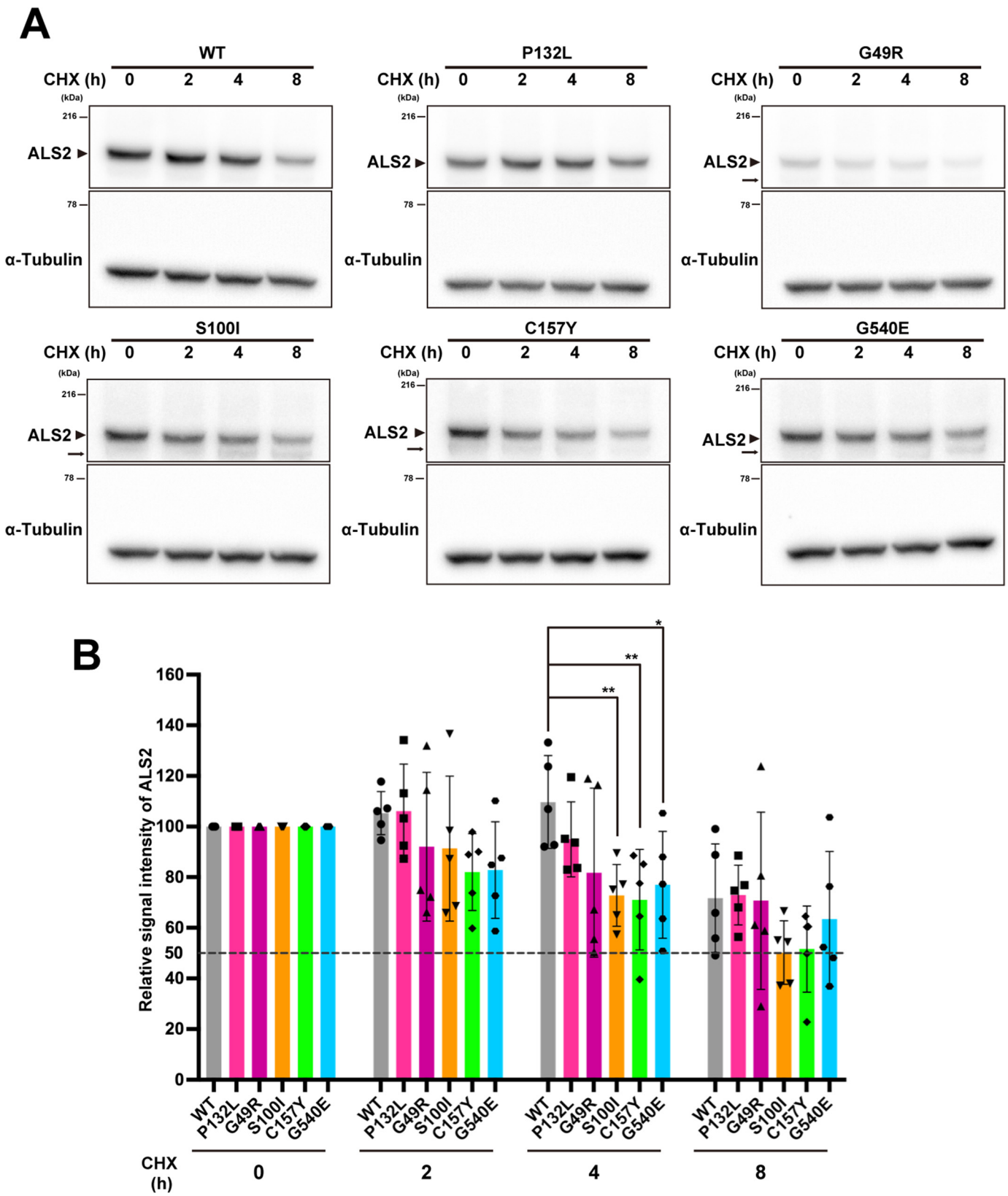

Figure 9. Analysis of the stability for ALS2 and its variants by the cycloheximide chase assay. *A,* Western blot analysis of FLAG-tagged ALS2 and its variants. NSC-34 cells that were transfected with pCIneoFLAG–ALS2^{WT}, pCIneoFLAG–ALS2^{P132L}, pCIneoFLAG–ALS2^{G49R}, pCIneoFLAG–ALS2^{S100I}, pCIneoFLAG–ALS2^{C157Y}, or pCIneoFLAG–ALS2^{G540E} were treated with CHX and harvested at different time points (0, 2, 4, and 8 h). Protein samples were analyzed by Western blotting using anti-ALS2–MORN/VPS9 and anti-α-tubulin antibodies. *Arrowheads* and *arrows* indicate ALS2 (184 kDa) and its degraded product, respectively. *B,* quantitative analysis of signal intensities for ALS2. Signal intensities were normalized by the level of α-tubulin. Value in each variant is presented as a mean (±S.D.) percentage relative to the respective signal intensity of ALS2 at 0 h ($n = 5$). Individual data points are also shown. Statistical significance was evaluated by two-way ANOVA with Bonferroni's multiple comparison test (*, $p < 0.05$; **, $p < 0.01$).

by the Mon1–Ccz1 heteromeric GEF complex (41). Furthermore, several Rho GEFs, including RasGRF1 (42), RasGRF2 (42), β1PIX (43, 44), Dbl (45), p115RhoGEF (46), PDZ-RhoGEF (46), and LARG (46), have been shown to form either dimer or oligomer, and such complex formation plays a crucial role in the GEF activities as well as their cellular functions. Consistent with these findings, we here demonstrated that ALS2 could form a tetramer in cells. Because there are no observable stable interactors other than ALS2 itself, the majority of ALS2 might exist as a homophilic tetramer in cells. Notably, the architecture of the ALS2 complex is well matched to that of the RIN2 complex, in which ALS2 tetramers are predicted to be assembled through the DH/PH domain-dependent self-interaction of two dimeric ALS2 complexes, each of which is interacted via the C-terminal MORN/VPS9 region in an antiparallel fashion (35, 39). Thus, it is reasonable to assume that tetrameric structure of the ALS2 complex might be crucial not only for the Rab5 activation but also for the intracellular localization as well as the functions of ALS2 (Fig. 10, *A* and *B*).

Previously, we have demonstrated that two pathogenic missense ALS2 variants, $ALS2^{C157Y}$ and $ALS2^{G540E}$, which retain the Rab5 GEF activity *in vitro*, can be recruited to membrane ruffles but fail to be relocalized to macropinosomes and/or early endosomes upon Rac1 activation, despite that macropinocytosis itself is activated (34). In this study, we further tested a single normal ALS2 variant and five additional missense or in-frame deletion pathogenic ALS2 variants, and we confirmed that all the pathogenic variants exhibited the same abnormal intracellular behaviors, irrespective of their residue positions of mutation, whereas normal ALS2 variant was normally relocalized to endosomes upon Rac1 activation. Then, we extended the analysis for the genotype (mutation)–phenotype (intracellular behaviors)–structural (complex) relationship (Table S2). Remarkably, the sizes of the ALS2 complex carrying missense mutations in the RLD or in-frame deletion in the central PH domain were shifted toward a higher molecular weight, indicating that these mutants formed extremely large ALS2 complexes in addition to normal tetramer. In contrast, the C-terminal VPS9 domain missense variants, $ALS2^{R1611W}$ and $ALS2^{L1617A}$, were rather present as dimeric or trimeric smaller forms in cells. More importantly, one of the artificial Rab5 GEF-defective mutants, $ALS2^{P1603A}$, not only primarily existed as a tetramer but also showed the endosomal localization in the presence of active Rac1, although it could not induce the fusion and enlargement of endosomes due to lack of the Rab5 GEF activity (34). These results suggest that the normal tetrameric structure of ALS2 might be requisite for the Rac1-induced relocalization of ALS2 from membrane ruffles to macropinosomes and/or endosome via macropinocytosis. Thus, a disorganized higher structure of the ALS2 complex is strongly implicated in the loss of cellular functions of ALS2 due to dysregulated intracellular behaviors of ALS2 and not just simply due to loss of Rab5 GEF activity.

One of the questions arising from this study includes the residue position-dependent differences in the oligomeric structures of ALS2. All the missense pathogenic mutations except for R1611W lead to form the larger complexes than normal tetramer, whereas ALS2 carrying the pathogenic mutation R1611W or the artificial mutation L1617A both exist as dimeric and/or trimeric smaller complexes. We have previously shown that the exon 25-deleted variant of ALS2 lacking the region spanning 1280–1335 aa completely lose the C-terminal region-mediated self-interaction of ALS2 (Table S2) (35). Because the C-terminal MORN/VPS9 region normally mediates the dimerization of ALS2, these particular missense mutations within the VPS9 domain may cause loss of proper dimerization of the C-terminal regions. Even though ALS2 loses the C-terminally-mediated dimerization property, ALS2 itself still can form some complex through the self-interactions between DH/PH and MORN/VPS9 and/or the RLD and MORN/VPS9 region (11, 35), resulting in the unusually smaller ALS2 complexes. By contrast, missense and small in-frame mutations in the RLD or PH domain may deregulate the normal assemble for the tetrameric complex of ALS2, thereby forming abnormally larger complexes of ALS2.

Another question arising from this study is how the structural distortion of the ALS2 complex leads to dysregulated intracellular ALS2 localization. Previously, we have demonstrated that two missense pathogenic full-length ALS2 variants, $ALS2^{C157Y}$ and $ALS2^{G540E}$, show a lower affinity to specific PIPs than does WT ALS2 (34). However, we showed here that the RLD fragment carrying the same missense mutations exhibited not only a similar pattern of affinities toward PIPs to those of the wildtype, but also the altered higher complex structure that was not associated with mutation itself. Importantly, *in silico* structure modeling demonstrated that missense pathogenic mutations in the RLD destabilized the normal protein structure, namely the architecture for a seven-bladed β-propeller. Indeed, the CHX chase assay in a motor neuron-like cell line revealed that some missense pathogenic mutations in the RLD destabilized the ALS2 protein. Because it is speculated that the RLD acts as a critical determinant for the intracellular localization of ALS2 (10), the structural distortion in the RLD might cause abnormal protein interactions between ALS2 and other regulators, thereby losing the normal intracellular behavior, in particular, the internalization of ALS2 via macropinocytosis (Fig. 10*C*).

Another possible explanation for the RLD-mediated regulation of intracellular ALS2 localization may be associated with the disordered region of the RLD. 306 aa of the intercalated disordered region (residues 219–524), which resides on the bottom surface of blade 5 of β-propeller, are predicted to contain several residues modified by phosphorylation, acetylation, and ubiquitylation (47). Furthermore, a database search identified two residues, Ser-483 and Ser-492, representing highly conserved phosphorylation sites (https://www.phosphosite.org/uniprotAccAction?id=Q96Q42)[3] (47). In fact, it has been reported that three residues in this region of ALS2, *i.e.* Ser-277, Ser-492, and Thr-510, are phosphorylated (48). We have previously demonstrated that the artificial ALS2 mutant carrying a single amino acid substitution on Thr-510 ($ALS2^{T510A}$) is properly relocalized to macropinosomes upon Rac1 activation (34), indicating the phosphorylation of Thr-510 may not have a

[3] Please note that the JBC is not responsible for the long-term archiving and maintenance of this site or any other third party hosted site.

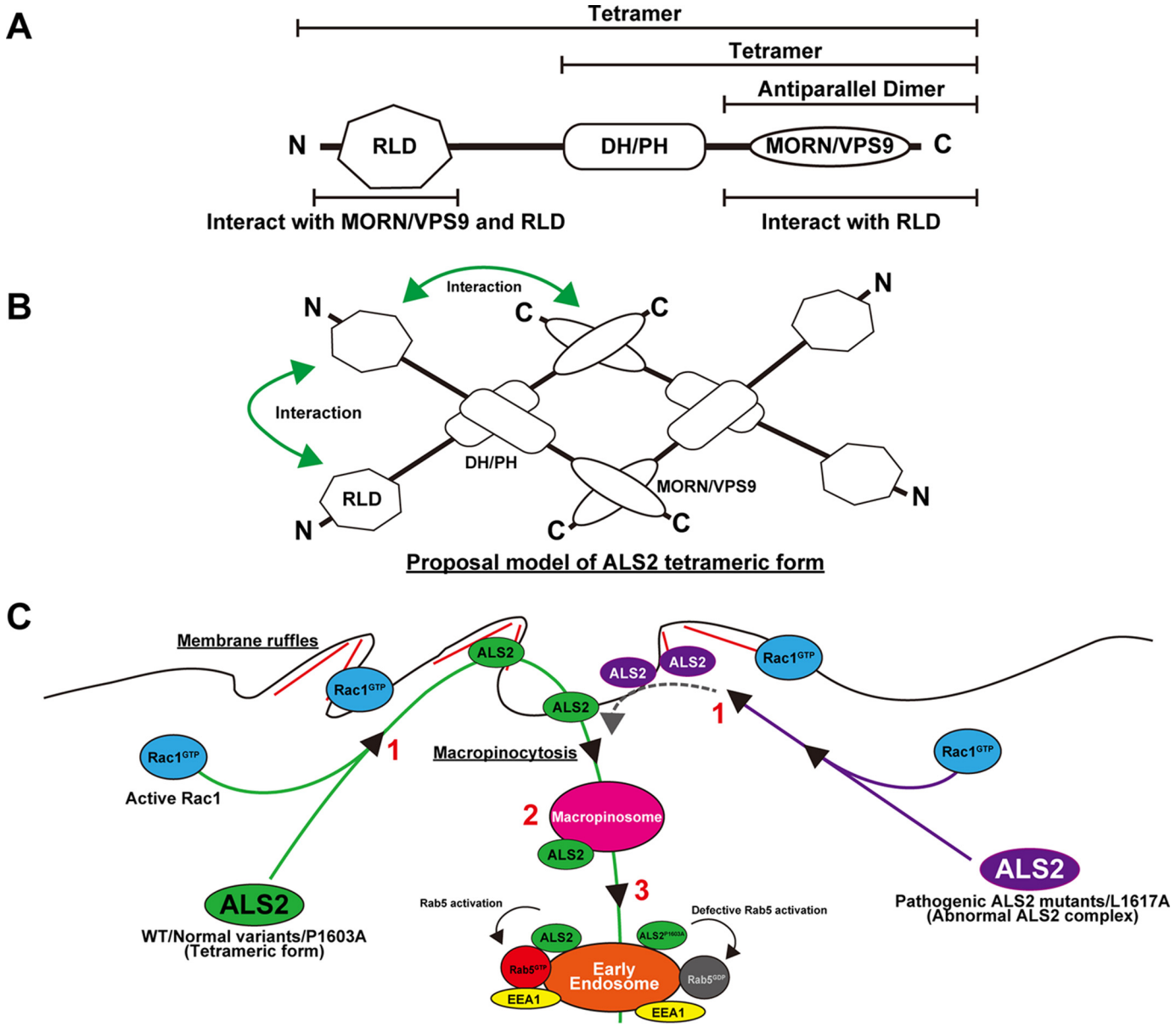

Figure 10. Proposed model for the oligomerization of ALS2 and a schematic diagram of intracellular distribution of WT ALS2 and mutant ALS2 complexes. *A*, self-interacting domains of ALS2. MORN/VPS9 forms an anti-parallel dimer and also can interact with RLD. DH/PH/MORN/VPS9 forms a tetramer through DH/PH. RLD can self-interact and also interact with MORN/VPS9. *B*, proposed model for the normal ALS2 tetramer. Four ALS2 molecules interact with each other in an anti-parallel fashion through MORN/VPS9 and DH/PH. RLDs can interact with each other and also with MORN/VPS9. *C*, intracellular distribution of the WT ALS2 and mutant ALS2 complexes. Rac1 activation induces the recruitment of ALS2 to membrane ruffles (indicated as *1*), followed by internalization to macropinosomes via macropinocytosis (indicated as *2*). Then, ALS2-inherent Rab5 GEF activity can facilitate the fusion of endosomal compartments (indicated as *3*). $ALS2^{WT}$, normal variant $ALS2^{P132L}$, and artificial mutant $ALS2^{P1603A}$, all of which can form a tetramer, are redistributed from the cytosol to endosomal compartments upon Rac1 activation and following macropinocytosis, whereas all pathogenic ALS2 mutants and artificial mutant $ALS2^{L1617A}$, all of which exist as the structurally-distorted complexes, fail to be loaded onto nascent macropinosomes on macropinocytosis and remain in ruffle membranes. It is noted that endosomal $ALS2^{P1603A}$ cannot mediate endosome fusion due to the defective Rab5 GEF activity.

major impact on the ALS2 localization. Currently, effects of other phosphorylated residues in the disordered region of the RLD remain to be investigated. Thus, to define the molecular mechanisms underlying the RLD-mediated intracellular localization of ALS2, future detailed studies will be required.

Recent molecular and cell biological studies have gradually been uncovering the molecular functions of ALS2 as well as their regulatory mechanisms: 1) oligomerization of the C-terminal MORN/VPS9 region of ALS2 is necessary for the activation of Rab5 (35); 2) ALS2-mediated Rab5 activation facilitates the fusion between macropinosome and endosomes and/or autophagosomes in cells (49, 50); 3) the intact DH/PH domain of ALS2 is indispensable for the redistribution of ALS2 to macropinosomes (11); and 4) active Rac1 induces the localization of ALS2 to membrane ruffles and then to macropinosome and/or endosomes via macropinocytosis (11). In this study, we have further revealed some additional regulatory mechanisms: 5) a tetrameric structure of ALS2 plays an essential role in Rac1-dependent endosomal localization of ALS2, and 6) mutations in the RLD distort the native tetrameric structure of ALS2, thereby losing the ability for the macropinocytosis-mediated internalization of ALS2. Such accumulating evidence allows us

to speculate that, under normal conditions, ALS2 acts as follows: Rac1 activation induces the conformational changes in the RLD by certain modifications on some residues, which in turn unlocked the RLD-mediated inhibitory switch; therefore, ALS2 can be recruited to membrane ruffles followed by internalization to macropinosomes via macropinocytosis. Ultimately, ALS2-inherent Rab5 GEF activity can facilitate the heterotypic as well as homotypic fusion of endosomal compartments. In the course of this dynamic signaling pathway, pathogenic ALS2 variants may become unresponsive to Rac1 signaling and/or fail to be loaded onto nascent macropinosomes on macropinocytosis due to the distorted complex structure, and thereby ALS2-mediated signaling might be disrupted (Fig. 10). However, further detailed studies are warranted to obtain direct evidence supporting these notions.

ALS2 is originally identified as a causative gene for autosomal recessive juvenile MNDs. Thus, loss of the ALS2 functions is believed to cause motor neuron degeneration. Concerning its lost functions, it has been shown that ALS2 is implicated in a variety of cellular processes and functions, including endosome fusion (10), macropinocytosis (11, 34, 49), autophagy (51), amphisome formation (50), neurite extension (49), receptor trafficking (52), mitochondrial morphology in neurons (53), and oxidative stress (53, 54). In addition, ALS2 is known to interact with many factors, including Rab5 (10), ALS2 C-terminal-like (ALS2CL) (55), glutamate receptor-interacting protein (GRIP) (52), and Rab17 (56). Most recently, NIMA-related expressed kinase 1 (NEK1), one of the important risk factors in sporadic as well as familial ALS, directly interact with ALS2 (57). Furthermore, molecular function of C9ORF72, a protein product of the most common causative ALS gene, is tightly associated with vesicle trafficking in the endolysosomal pathway (58, 59), where ALS2 functions in cells. Deciphering such intricate molecular systems regulated by ALS2 along with other interactors and/or regulators is still a formidable task. However, our data might provide important clues to understand not only the normal function of ALS2 but also molecular mechanisms underlying the pathogenesis of *ALS2*-linked MNDs.

Experimental procedures

Antibodies and materials

Anti-ALS2–RLD (HPF1–680) and anti-ALS2–MORN/VPS9 (MPF1012–1651) polyclonal antibodies were described previously (10). Monoclonal antibodies used in this study included anti-FLAG M2 (Sigma), anti-HA (Cell Signaling Technology), anti-EEA1 (BD Biosciences), and anti-α-tubulin polyclonal HRP-DirecT (MBL) antibodies. All other regents were from commercial sources and of analytical used grade.

Plasmid constructs

The expression constructs, including pGEX6P–ALS2–RLD^{WT}, pGEX6P–ALS2–MORN/VPS9^{WT}, pCIneoFLAG–ALS2–RLD^{WT}, pCIneoFLAG–ALS2–MORN/VPS9^{WT}, pCIneoFLAG–ALS2^{WT}, pCIneoHA–ALS2^{WT}, pCIneoFLAG–ALS2^{C157Y}, pCIneoHA–ALS2^{C157Y}, pCIneoFLAG–ALS2^{G540E}, pCIneoHA–ALS2^{G540E}, pCIneoFLAG–ALS2^{P1603A}, pCIneoFLAG–ALS2^{L1617A}, pCMV10-2xHA-Rac1^{Q61L}, and pCIneoFLAG-EEA1, were described previously (10, 11, 34, 35). In addition to these constructs, we generated pCIneoFLAG–ALS2–RLD^{S100I}, pCIneoFLAG–ALS2–RLD^{P132L}, pCIneoFLAG–ALS2–RLD^{C157Y}, pCIneoFLAG–ALS2–RLD^{G540E}, pCIneoFLAG–ALS2^{S100I}, pCIneoHA–ALS2^{S100I}, pCIneoFLAG–ALS2^{P132L}, pCIneoFLAG–ALS2^{A861_T904del}, pCIneoHA–ALS2^{A861_T904del}, pCIneoFLAG–ALS2^{E1173K}, pCIneoFLAG–ALS2^{R1611W}, and pCIneoHA–ALS2^{R1611W} by the site-directed mutagenesis using pCIneoFLAG–ALS2–RLD^{WT} or pCIneo–FLAG–ALS2^{WT} as a template. The insert DNA of these constructs were verified by DNA sequence analysis.

Cell culture and transfection

HeLa, COS-7 and NSC-34 (CELLutions Biosystems) cells were cultured in Dulbecco's modified Eagle's medium with high glucose (Wako) supplemented with 10% heat-inactivated fetal bovine serum gold (PAA Laboratories GmbH), 100 units/ml penicillin, 100 μg/ml streptomycin, and 1 mM sodium pyruvate. Cells were transfected with plasmid constructs using the Effectene Transfection Reagent (Qiagen) according to the manufacturer's instructions. NSC-34 cells were transfected with plasmid constructs using the Lipofectamine^{TM} 3000 transfection reagent (ThermoFisher Scientifc) (33).

Immunocytochemistry and confocal microscopy

Immunofluorescence studies were carried out as described previously (11, 34). Briefly, HeLa cells transfected with appropriate plasmids were washed with PBS(−) twice, fixed with 4% paraformaldehyde in PBS(−) for 20 min, and permeabilized with 0.1% Triton X-100 and 5% normal goat serum (NGS) in PBS(−) for 30 min. Anti-ALS2–RLD (1:10,000) and anti-EEA1 (1:100) antibodies diluted in PBS(−) containing 0.05% Triton X-100 and 1% NGS were added to the fixed cells and incubated overnight (overnight) at room temperature. After washing with PBS(−) (10 min, three times), samples were incubated with Alexa 488- or 594-conjugated anti-mouse or -rabbit IgG (Molecular Probes) (1:500) in 0.05% Triton X-100 and 1% NGS/PBS(−). F-actin was visualized by Alexa 594-conjugated phalloidin (Molecular Probes) (1:500) in 0.05% Triton X-100 and 1% NGS/PBS(−). After washing with PBS(−), the cells were mounted with Vectashield with 4′,6-diamidino-2-phenylindole dihydrochloride. We observed these cells by Leica TCS_NT (Leica) confocal microscope system and ZEISS LSM-700 laser scanning confocal microscope (Carl Zeiss). Images were quantified using ImageJ software.

Dextran uptake assay and line plot profile

HeLa cells were transfected with pCIneoFLAG–ALS2^{WT}, pCIneoFLAG–ALS2^{S100I}, pCIneoFLAG–ALS2^{A861_T904del}, or pCIneoFLAG–ALS2^{R1611W} together with or without pCMV10-2xHA–Rac1^{Q61L} as described previously (34). Twenty four hours after transfection, the cells were washed with PBS(−) and cultured in serum-free Dulbecco's modified Eagle's medium containing 2 mg/ml tetramethylrhodamine-conjugated dextran MW 70,000, lysine-fixable (Invitrogen) for 20 min. After washing with PBS(−), the cells were fixed and observed by Zeiss LSM-700 laser-scanning confocal microscope (Carl Zeiss). Captured cell images were further subjected to the line-analysis

by drawing two cross-sectional lines (each 16 μm in length) per macropinosome using RBG profile plot in ImageJ software.

Preparation and purification of FLAG-tagged ALS2 protein

COS-7 cells were transfected with pCIneoFLAG–ALS2 constructs. Twenty four hours after transfection, the cells were washed with PBS(−) and lysed in buffer A (50 mM Tris-HCl (pH 7.5), 150 mM NaCl, 1% Tween 20, and Complete Protease Inhibitor (Roche Diagnostics)). After centrifugation at 23,000 × *g* for 20 min, supernatants were recovered and subjected to gel-filtration chromatography. Resulting supernatants were further subjected to immunoprecipitation with anti-FLAG M2 affinity gel (Sigma). The affinity gels were washed three times with buffer B (20 mM Tris-HCl (pH 7.5), 150 mM NaCl containing 1% Tween 20). Subsequently, the affinity gels were treated with 100 μg/ml 3xFLAG peptide (Sigma) for 30 min at room temperature, and FLAG-tagged ALS2 was eluted. After centrifugation, eluates were subjected to silver staining using Sil-Best Stain One (Nacalai Tesque) according to the manufacturer's instructions.

Purification of GST-fused ALS2 protein

GST-fused ALS2–RLD^{WT} and ALS2–MORN/VPS9^{WT} were expressed in *Escherichia coli* BL21(DE3) pLys S (Novagen) cells, which were transformed with pGEX6P–ALS2–RLD^{WT} and pGEX6P–ALS2–MORN/VPS9^{WT}, respectively, in LB medium containing 100 μM isopropyl thio-β-D-galactoside overnight at 37 °C. *E. coli* pellets were lysed in buffer C (20 mM Tris-HCl (pH 7.5), 150 mM NaCl, 0.1% IGEPAL® CA-630 (Sigma) and Complete Protease Inhibitor (Roche Diagnostics)). After centrifugation at 20,000 × *g* for 30 min, supernatants were mixed with GSH-Sepharose™ 4B beads (Amersham Biosciences). After washing with buffer C, GST-fused proteins were treated with Pre-Scission protease buffer (50 mM Tris-HCl (pH 7.5), 100 mM NaCl, 1 mM EDTA, 1 mM DTT, Pre-Scission protease (Amersham Biosciences)) to remove the GST moiety according to the manufacturer's recommendations. Purified proteins were subjected to gel-filtration chromatography.

Western blot analysis

Protein samples were separated by SDS-PAGE (Wako Supersep™ Ace, 5–20% 17-well) and blotted onto polyvinylidene difluoride membranes (Bio-Rad or Merck Millipore Immobilin-P). The blots were blocked with 0.5% skimmed milk in TBST (20 mM Tris-HCl (pH 7.5), 150 mM NaCl containing 0.1% Tween 20) for 1 h at room temperature. The blocked membrane was incubated with anti-ALS2–RLD (1:5000), anti-ALS2–MORN/VPS9 (1:5000), anti-FLAG M2 (1:1000), anti-HA (1:2000), or HRP-conjugated-anti-α-tubulin (1:10,000) antibody overnight at room temperature. After washing with TBST (15 min, 4 times), membranes were incubated with HRP-conjugated anti-rabbit (1:5000) or anti-mouse (1:5000) secondary antibody (GE Healthcare) in TBST for 2 h at room temperature. After washing with TBST, immunoreactive protein bands were visualized by Immobilon® Western HRP (Merck Millipore) and detected by Ez-Capture MG (ATTO).

Coimmunoprecipitation

Coimmunoprecipitation experiments were carried out as described previously (34). In brief, COS-7 cells were transfected with pCIneoFLAG–ALS2 and pICneoHA–ALS2 constructs. Twenty four hours after transfection, the cells were lysed in buffer A (50 mM Tris-HCl (pH 7.5), 150 mM NaCl, 1% Tween 20, and Complete protease inhibitor (Roche Diagnostics)). Supernatants were recovered by centrifugation at 23,000 × *g* for 20 min. Immunoprecipitation (IP) was performed by using anti-FLAG M2 affinity gel (Sigma). The FLAG M2 affinity gels were washed with buffer B (20 mM Tris-HCl (pH 7.5), 150 mM NaCl containing 1% Tween 20). IP products were subjected to Western blot analysis with either the anti-FLAG M2 or anti-HA antibody.

Gel-filtration chromatography

COS-7 cells were transfected with pCIneoFLAG–ALS2 constructs. Twenty four hours after transfection, the cells were washed with PBS(−) and lysed in buffer D (50 mM Tris-HCl (pH 7.5), 150 mM NaCl, 0.1% IGEPAL CA-630 (Sigma), and Complete protease inhibitor (Roche Diagnostics)). Supernatants were recovered by centrifugation at 23,000 × *g* for 20 min and loaded onto the column (Superose 6 10/300 GE Healthcare), and the eluates were fractionated and collected. Elution was carried out at 4 °C at a flow rate of 0.3 ml/min with a fraction volume of 0.5 ml. Fractionated samples were analyzed by Western blotting using the anti-ALS2–MORN/VPS9 or anti-ALS2-RLD antibody. The elution profile of the column was calibrated with the size standards (IgM, 975 kDa; thyroglobulin, 669 kDa; ferritin, 440 kDa; aldolase, 158 kDa; and ovalbumin, 43 kDa).

Quantification of signal intensities on Western blotting for gel-filtration chromatography

Signal intensities of Western blots were quantified by using CS Analyzer Version 3.0 (ATTO), and each fraction was expressed as a percentage of the total signal intensities from protein bands of interest within the entire fractions.

Protein–lipid overlay assay

PIPs overlay assay of FLAG-fused proteins was conducted according to the manufacturer's instructions. In brief, PIP Strips™ (100 pmol per spot) (Echelon Biosciences) were incubated with 0.2 μg/ml purified FLAG–ALS2-RLD^{WT}, FLAG–ALS2–RLD^{S100I}, FLAG–ALS2^{P132L}, FLAG–ALS2–RLD^{C157Y}, or FLAG–ALS2–RLD^{G540E} in TBST containing 3% (w/v) of fatty acid-free BSA (Sigma) overnight at 4 °C. FLAG peptides purified from the cell lysate of empty vector-transfected cells were used as a control. PIP strips™ (Echelon Biosciences, Inc.) were washed and incubated with anti-ALS2–RLD antibody (1:5000) for 2 h at room temperature. After washing with TBST, membranes were incubated with HRP-conjugated anti-rabbit secondary antibody (1:5000) (GE Healthcare) in TBST for 2 h at room temperature. After washing with TBST, immunoreactive protein spots were visualized by Immobilon® Western HRP (Merck Millipore) and detected by Ez-Capture MG (ATTO). Signal intensities of PIP strips™ were quantified by using CS Analyzer Version 3.0 (ATTO). Each value was expressed as a

percentage of the total signal intensities from all the spots within the entire strip.

Homology modeling

Amino acid sequence of the RLD of human ALS2 (ALS2–RLD) (GenBank™ accession no. BAB69014) was obtained from NCBI GenBank™ database and used as a target for homology modeling. After BLASTP searches against Protein Data Bank (PDB) sequence entries using ALS2–RLD sequence as a query, the third RLD of human HERC2 (PDB code 3KCI) was selected as the best template for homology modeling (Bit score: 115.2 and Identity: 32%). The 3KCI structure was optimized for inserting missing atoms in incomplete residues, modeling missing loop regions, and deleting alternative conformations by the Prepare Protein protocol. The template and target amino acid sequences were first aligned. Then, the quality of the alignment was improved by removing gaps, particularly 306 aa of the intercalated disordered sequence (residues 219–524), and realigning the sequence, and we generated 50 structure models of the RLD of ALS2 using a Build Homology Models protocol/MODELLER (60) in Discovery Studio version 4.1 from BIOVIA (Accelrys Inc. San Diego). The Probability Density Function total energy and Discrete Optimized Potential Energy score were used to select the best model. The loops in the resulting model were refined using the protocol Loop Refinement. The Ramachandran plots and Verify 3D in Discovery Studio were also used for the model evaluation. A CHARMm force field implemented in Discovery Studio was typed for the simulation.

Structural analysis of RCC1-like domain of ALS2

The structural models of ALS2 mutants were built based on optimized models using the Build Mutants protocol of the Macromolecular tool. To optimize the conformation of both the mutated and neighboring residues surrounding mutations, the cut radius (4.5Å) was used in this simulation. Protein stabilities for mutants were calculated using a Calculate Mutation Energy (Stability) protocol. All molecular modeling, optimization, and visualization were performed in Discovery Studio with default parameter setting. The surface hydrophobicity (61) of a residue was calculated in a 3-amino acid window and was drawn using Discovery Studio.

Cycloheximide chase assay

NSC-34 cells were transfected with pCIneoFLAG–ALS2^{WT}, pCIneoFLAG–ALS2^{P132L}, pCIneoFLAG–ALS2^{G49R}, pCIneoFLAG–ALS2^{S100I}, pCIneoFLAG–ALS2^{C157Y}, or pCIneoFLAG–ALS2^{G540E} construct. Twenty four hours after transfection, the cells were washed with PBS(−), followed by the incubation with Dulbecco's modified Eagle's medium containing 50 μg/ml CHX (Calbiochem). CHX-treated cells were harvested at different time points (0, 2, 4, and 8 h) and lysed in buffer A. Supernatants were recovered by centrifugation at 23,000 × *g* for 20 min and analyzed by Western blotting using the anti-ALS2–MORN/VPS9 antibody and anti-α-tubulin antibody as an internal control.

Statistical analysis

Statistical analyses were conducted using Prism 7 (GraphPad). Statistical significances for signal intensities on Western blotting for gel-filtration chromatography or PIPs strip membrane for protein lipid overlay assay were evaluated by one-way ANOVA with Bonferroni's multiple comparison tests. Signal intensities on Western blotting for the CHX chase assay were evaluated by two-way ANOVA with Bonferroni's multiple comparison tests. A p value <0.05 was considered as reaching statistical significance.

Author contributions—K. S., A. O., M. T. U., H.-F. S., and S. H. conceptualization; K. S., A. O., M. T. U., Y. H., K. S.-U., J. S., and S. H. resources; K. S., A. O., M. T. U., Y. H., K. S.-U., J. S., S. Murakoshi, S. Mitsui, S.O., and S. N. data curation; K. S., A. O., M. T. U., Y. H., K. S.-U., J. S., S. Mitsui, S. O., and S. N. formal analysis; S. H. supervision; H.-F. S. and S. H. funding acquisition; K. S., A. O., M. T. U., Y. H., K. S.-U., J. S., S. Murakoshi, S. Mitsui, S. O., S. N., and H.-F. S. investigation; K. S., A. O., M. T. U., and Y. H. visualization; K. S., A. O., M. T. U., Y. H., and S. N. methodology; K. S., A. O., M. T. U., and S. H. writing-original draft; H.-F. S. and S. H. project administration; K. S., A. O., M. T. U., Y. H., S. N., H.-F. S., and S. H. writing-review and editing; A. O., M. T. U., S. Mitsui, S. O., and S. N. validation; M. T. U. and S. O. software.

Acknowledgments—We thank Hideo Tsukamoto, Ayumi Sasaki, Chisa Okada, and all other members of Support Center for Medical Research and Education at Tokai University for their technical help. We also thank Prof. Joh-E. Ikeda (Ottawa University) for invaluable and generous support.

References

1. Hadano, S., Hand, C. K., Osuga, H., Yanagisawa, Y., Otomo, A., Devon, R. S., Miyamoto, N., Showguchi-Miyata, J., Okada, Y., Singaraja, R., Figlewicz, D. A., Kwiatkowski, T., Hosler, B. A., Sagie, T., Skaug, J., *et al.* (2001) A gene encoding a putative GTPase regulator is mutated in familial amyotrophic lateral sclerosis 2. *Nat. Genet.* **29,** 166–173 CrossRef Medline
2. Yang, Y., Hentati, A., Deng, H. X., Dabbagh, O., Sasaki, T., Hirano, M., Hung, W. Y., Ouahchi, K., Yan, J., Azim, A. C., Cole, N., Gascon, G., Yagmour, A., Ben-Hamida, M., Pericak-Vance, M., *et al.* (2001) The gene encoding alsin, a protein with three guanine-nucleotide exchange factor domains, is mutated in a form of recessive amyotrophic lateral sclerosis. *Nat. Genet.* **29,** 160–165 CrossRef Medline
3. Ben Hamida, M., Hentati, F., and Ben Hamida, C. (1990) Hereditary motor system diseases (chronic juvenile amyotrophic lateral sclerosis). Conditions combining a bilateral pyramidal syndrome with limb and bulbar amyotrophy. *Brain* **113,** 347–363 CrossRef Medline
4. Eymard-Pierre, E., Lesca, G., Dollet, S., Santorelli, F. M., di Capua, M., Bertini, E., and Boespflug-Tanguy, O. (2002) Infantile-onset ascending hereditary spastic paralysis is associated with mutations in the alsin gene. *Am. J. Hum. Genet.* **71,** 518–527 CrossRef Medline
5. Devon, R. S., Helm, J. R., Rouleau, G. A., Leitner, Y., Lerman-Sagie, T., Lev, D., and Hayden, M. R. (2003) The first nonsense mutation in alsin results in a homogeneous phenotype of infantile-onset ascending spastic paralysis with bulbar involvement in two siblings. *Clin. Genet.* **64,** 210–215 CrossRef Medline
6. Rosa, J. L., Casaroli-Marano, R. P., Buckler, A. J., Vilaró, S., and Barbacid, M. (1996) p619, a giant protein related to the chromosome condensation regulator RCC1, stimulates guanine nucleotide exchange on ARF1 and Rab proteins. *EMBO J.* **15,** 4262–4273 CrossRef Medline
7. Schmidt, A., and Hall, A. (2002) Guanine nucleotide exchange factors for Rho GTPases: turning on the switch. *Genes Dev.* **16,** 1587–1609 CrossRef Medline
8. Carney, D. S., Davies, B. A., and Horazdovsky, B. F. (2006) Vps9 domain-containing proteins: activators of Rab5 GTPases from yeast to neurons. *Trends Cell Biol.* **16,** 27–35 CrossRef Medline

9. Takeshima, H., Komazaki, S., Nishi, M., Iino, M., and Kangawa, K. (2000) Junctophilins: a novel family of junctional membrane complex proteins. *Mol. Cell* **6,** 11–22 CrossRef Medline
10. Otomo, A., Hadano, S., Okada, T., Mizumura, H., Kunita, R., Nishijima, H., Showguchi-Miyata, J., Yanagisawa, Y., Kohiki, E., Suga, E., Yasuda, M., Osuga, H., Nishimoto, T., Narumiya, S., and Ikeda, J. E. (2003) ALS2, a novel guanine nucleotide exchange factor for the small GTPase Rab5, is implicated in endosomal dynamics. *Hum. Mol. Genet.* **12,** 1671–1687 CrossRef Medline
11. Kunita, R., Otomo, A., Mizumura, H., Suzuki-Utsunomiya, K., Hadano, S., and Ikeda, J. E. (2007) The Rab5 activator ALS2/alsin acts as a novel Rac1 effector through Rac1-activated endocytosis. *J. Biol. Chem.* **282,** 16599–16611 CrossRef Medline
12. Flor-de-Lima, F., Sampaio, M., Nahavandi, N., Fernandes, S., and Leão, M. (2014) Alsin related disorders: literature review and case study with novel mutations. *Case Rep. Genet.* **2014,** 691515 Medline
13. Daud, S., Kakar, N., Goebel, I., Hashmi, A. S., Yaqub, T., Nürnberg, G., Nürnberg, P., Morris-Rosendahl, D. J., Wasim, M., Volk, A. E., Kubisch, C., Ahmad, J., and Borck, G. (2016) Identification of two novel ALS2 mutations in infantile-onset ascending hereditary spastic paraplegia. *Amyotroph. Lateral Scler. Frontotemporal Degener.* **17,** 260–265 CrossRef Medline
14. Luigetti, M., Lattante, S., Conte, A., Romano, A., Zollino, M., Marangi, G., and Sabatelli, M. (2013) A novel compound heterozygous ALS2 mutation in two Italian siblings with juvenile amyotrophic lateral sclerosis. *Amyotroph. Lateral Scler. Frontotemporal Degener.* **14,** 470–472 CrossRef Medline
15. Shi, Y., Hirano, Y. Y., and Siddique, N. (2012) Five novel mutations in alsin gene in juvenile ALS and juvenile PLS individuals. *Amyotrophic Lateral Sclerosis* **13,** 111–125 CrossRef
16. Eymard-Pierre, E., Yamanaka, K., Haeussler, M., Kress, W., Gauthier-Barichard, F., Combes, P., Cleveland, D. W., and Boespflug-Tanguy, O. (2006) Novel missense mutation in ALS2 gene results in infantile ascending hereditary spastic paralysis. *Ann. Neurol.* **59,** 976–980 CrossRef Medline
17. Kress, J. A., Kühnlein, P., Winter, P., Ludolph, A. C., Kassubek, J., Müller, U., and Sperfeld, A. D. (2005) Novel mutation in the ALS2 gene in juvenile amyotrophic lateral sclerosis. *Ann. Neurol.* **58,** 800–803 CrossRef Medline
18. Nishiyama, A., Niihori, T., Warita, H., Izumi, R., Akiyama, T., Kato, M., Suzuki, N., Aoki, Y., and Aoki, M. (2017) Comprehensive targeted next-generation sequencing in Japanese familial amyotrophic lateral sclerosis. *Neurobiol. Aging* **53,** 194.e1–194.e8 CrossRef Medline
19. Xie, F., Cen, Z. D., Xiao, J. F., and Luo, W. (2015) Novel compound heterozygous ALS2 mutations in two Chinese siblings with infantile ascending hereditary spastic paralysis. *Neurol. Sci.* **36,** 1279–1280 CrossRef Medline
20. Panzeri, C., De Palma, C., Martinuzzi, A., Daga, A., De Polo, G., Bresolin, N., Miller, C. C., Tudor, E. L., Clementi, E., and Bassi, M. T. (2006) The first ALS2 missense mutation associated with JPLS reveals new aspects of alsin biological function. *Brain* **129,** 1710–1719 CrossRef Medline
21. Sztriha, L., Panzeri, C., Kálmánchey, R., Szabó, N., Endreffy, E., Túri, S., Baschirotto, C., Bresolin, N., Vekerdy, Z., and Bassi, M. T. (2008) First case of compound heterozygosity in ALS2 gene in infantile-onset ascending spastic paralysis with bulbar involvement. *Clin. Genet.* **73,** 591–593 CrossRef Medline
22. Tariq, H., Mukhtar, S., and Naz, S. (2017) A novel mutation in ALS2 associated with severe and progressive infantile onset of spastic paralysis. *J. Neurogenet.* **31,** 26–29 CrossRef Medline
23. Herzfeld, T., Wolf, N., Winter, P., Hackstein, H., Vater, D., and Müller, U. (2009) Maternal uniparental heterodisomy with partial isodisomy of a chromosome 2 carrying a splice acceptor site mutation (IVS9–2A→T) in ALS2 causes infantile-onset ascending spastic paralysis (IAHSP). *Neurogenetics* **10,** 59–64 CrossRef Medline
24. Sheerin, U. M., Schneider, S. A., Carr, L., Deuschl, G., Hopfner, F., Stamelou, M., Wood, N. W., and Bhatia, K. P. (2014) ALS2 mutations: juvenile amyotrophic lateral sclerosis and generalized dystonia. *Neurology* **82,** 1065–1067 CrossRef Medline
25. Verschuuren-Bemelmans, C. C., Winter, P., Sival, D. A., Elting, J. W., Brouwer, O. F., and Müller, U. (2008) Novel homozygous ALS2 nonsense mutation (p.Gln715X) in sibs with infantile-onset ascending spastic paralysis: the first cases from northwestern Europe. *Eur. J. Hum. Genet.* **16,** 1407–1411 CrossRef Medline
26. Eker, H. K., Unlü, S. E., Al-Salmi, F., and Crosby, A. H. (2014) A novel homozygous mutation in ALS2 gene in four siblings with infantile-onset ascending hereditary spastic paralysis. *Eur. J. Med. Genet.* **57,** 275–278 CrossRef Medline
27. Wakil, S. M., Ramzan, K., Abuthuraya, R., Hagos, S., Al-Dossari, H., Al-Omar, R., Murad, H., Chedrawi, A., Al-Hassnan, Z. N., Finsterer, J., and Bohlega, S. (2014) Infantile-onset ascending hereditary spastic paraplegia with bulbar involvement due to the novel ALS2 mutation c.2761C→T. *Gene* **536,** 217–220 CrossRef Medline
28. Mintchev, N., Zamba-Papanicolaou, E., Kleopa, K. A., and Christodoulou, K. (2009) A novel ALS2 splice-site mutation in a Cypriot juvenile-onset primary lateral sclerosis family. *Neurology* **72,** 28–32 CrossRef Medline
29. Siddiqi, S., Foo, J. N., Vu, A., Azim, S., Silver, D. L., Mansoor, A., Tay, S. K., Abbasi, S., Hashmi, A. H., Janjua, J., Khalid, S., Tai, E. S., Yeo, G. W., and Khor, C. C. (2014) A novel splice-site mutation in ALS2 establishes the diagnosis of juvenile amyotrophic lateral sclerosis in a family with early onset anarthria and generalized dystonias. *PLoS ONE* **9,** e113258 CrossRef Medline
30. Shirakawa, K., Suzuki, H., Ito, M., Kono, S., Uchiyama, T., Ohashi, T., and Miyajima, H. (2009) Novel compound heterozygous ALS2 mutations cause juvenile amyotrophic lateral sclerosis in Japan. *Neurology* **73,** 2124–2126 CrossRef Medline
31. Racis, L., Tessa, A., Pugliatti, M., Storti, E., Agnetti, V., and Santorelli, F. M. (2014) Infantile-onset ascending hereditary spastic paralysis: a case report and brief literature review. *Eur. J. Paediatr. Neurol.* **18,** 235–239 CrossRef Medline
32. Gros-Louis, F., Meijer, I. A., Hand, C. K., Dubé, M. P., MacGregor, D. L., Seni, M. H., Devon, R. S., Hayden, M. R., Andermann, F., Andermann, E., and Rouleau, G. A. (2003) An ALS2 gene mutation causes hereditary spastic paraplegia in a Pakistani kindred. *Ann. Neurol.* **53,** 144–145 CrossRef Medline
33. Yamanaka, K., Vande Velde, C., Eymard-Pierre, E., Bertini, E., Boespflug-Tanguy, O., and Cleveland, D. W. (2003) Unstable mutants in the peripheral endosomal membrane component ALS2 cause early-onset motor neuron disease. *Proc. Natl. Acad. Sci. U.S.A.* **100,** 16041–16046 CrossRef Medline
34. Otomo, A., Kunita, R., Suzuki-Utsunomiya, K., Ikeda, J. E., and Hadano, S. (2011) Defective relocalization of ALS2/alsin missense mutants to Rac1-induced macropinosomes accounts for loss of their cellular function and leads to disturbed amphisome formation. *FEBS Lett.* **585,** 730–736 CrossRef Medline
35. Kunita, R., Otomo, A., Mizumura, H., Suzuki, K., Showguchi-Miyata, J., Yanagisawa, Y., Hadano, S., and Ikeda, J. E. (2004) Homo-oligomerization of ALS2 through its unique carboxyl-terminal regions is essential for the ALS2-associated Rab5 guanine nucleotide exchange activity and its regulatory function on endosome trafficking. *J. Biol. Chem.* **279,** 38626–38635 CrossRef Medline
36. Hadano, S., and Ikeda, J. E. (2005) Purification and functional analyses of ALS2 and its homologue. *Methods Enzymol.* **403,** 310–321 CrossRef Medline
37. Egami, Y., Taguchi, T., Maekawa, M., Arai, H., and Araki, N. (2014) Small GTPases and phosphoinositides in the regulatory mechanisms of macropinosome formation and maturation. *Front. Physiol.* **5,** 374 Medline
38. Stenmark, H., Vitale, G., Ullrich, O., and Zerial, M. (1995) Rabaptin-5 is a direct effector of the small GTPase Rab5 in endocytic membrane fusion. *Cell* **83,** 423–432 CrossRef Medline
39. Saito, K., Murai, J., Kajiho, H., Kontani, K., Kurosu, H., and Katada, T. (2002) A novel binding protein composed of homophilic tetramer exhibits unique properties for the small GTPase Rab5. *J. Biol. Chem.* **277,** 3412–3418 CrossRef Medline
40. Saito, K., Kajiho, H., Araki, Y., Kurosu, H., Kontani, K., Nishina, H., and Katada, T. (2005) Purification and analysis of RIN family-novel Rab5 GEFs. *Methods Enzymol.* **403,** 276–283 CrossRef Medline

41. Nordmann, M., Cabrera, M., Perz, A., Bröcker, C., Ostrowicz, C., Engelbrecht-Vandré, S., and Ungermann, C. (2010) The Mon1–Ccz1 complex is the GEF of the late endosomal Rab7 homolog Ypt7. *Curr. Biol.* **20,** 1654–1659 CrossRef Medline
42. Anborgh, P. H., Qian, X., Papageorge, A. G., Vass, W. C., DeClue, J. E., and Lowy, D. R. (1999) Ras-specific exchange factor GRF: oligomerization through its Dbl homology domain and calcium-dependent activation of Raf. *Mol. Cell. Biol.* **19,** 4611–4622 CrossRef Medline
43. Koh, C. G., Manser, E., Zhao, Z. S., Ng, C. P., and Lim, L. (2001) Beta1PIX, the PAK-interacting exchange factor, requires localization via a coiled-coil region to promote microvillus-like structures and membrane ruffles. *J. Cell Sci.* **114,** 4239–4251 Medline
44. Kim, S., Lee, S. H., and Park, D. (2001) Leucine zipper-mediated homodimerization of the p21-activated kinase-interacting factor, βPix. Implication for a role in cytoskeletal reorganization. *J. Biol. Chem.* **276,** 10581–10584 CrossRef Medline
45. Zhu, K., Debreceni, B., Bi, F., and Zheng, Y. (2001) Oligomerization of DH domain is essential for Dbl-induced transformation. *Mol. Cell. Biol.* **21,** 425–437 CrossRef Medline
46. Chikumi, H., Barac, A., Behbahani, B., Gao, Y., Teramoto, H., Zheng, Y., and Gutkind, J. S. (2004) Homo- and hetero-oligomerization of PDZ-RhoGEF, LARG and p115RhoGEF by their C-terminal region regulates their *in vivo* Rho GEF activity and transforming potential. *Oncogene* **23,** 233–240 CrossRef Medline
47. Hornbeck, P. V., Zhang, B., Murray, B., Kornhauser, J. M., Latham, V., and Skrzypek, E. (2015) PhosphoSitePlus, 2014: mutations, PTMs and recalibrations. *Nucleic Acids Res.* **43,** D512–D520 CrossRef Medline
48. Tudor, E. L., Perkinton, M. S., Schmidt, A., Ackerley, S., Brownlees, J., Jacobsen, N. J., Byers, H. L., Ward, M., Hall, A., Leigh, P. N., Shaw, C. E., McLoughlin, D. M., and Miller, C. C. (2005) ALS2/Alsin regulates Rac-PAK signaling and neurite outgrowth. *J. Biol. Chem.* **280,** 34735–34740 CrossRef Medline
49. Otomo, A., Kunita, R., Suzuki-Utsunomiya, K., Mizumura, H., Onoe, K., Osuga, H., Hadano, S., and Ikeda, J. E. (2008) ALS2/alsin deficiency in neurons leads to mild defects in macropinocytosis and axonal growth. *Biochem. Biophys. Res. Commun.* **370,** 87–92 CrossRef Medline
50. Hadano, S., Otomo, A., Kunita, R., Suzuki-Utsunomiya, K., Akatsuka, A., Koike, M., Aoki, M., Uchiyama, Y., Itoyama, Y., and Ikeda, J. E. (2010) Loss of ALS2/Alsin exacerbates motor dysfunction in a SOD1-expressing mouse ALS model by disturbing endolysosomal trafficking. *PLoS ONE* **5,** e9805 CrossRef Medline
51. Hadano, S., Mitsui, S., Pan, L., Otomo, A., Kubo, M., Sato, K., Ono, S., Onodera, W., Abe, K., Chen, X., Koike, M., Uchiyama, Y., Aoki, M., Warabi, E., Yamamoto, M., Ishii, T., *et al.* (2016) Functional links between SQSTM1 and ALS2 in the pathogenesis of ALS: cumulative impact on the protection against mutant SOD1-mediated motor dysfunction in mice. *Hum. Mol. Genet.* **25,** 3321–3340 CrossRef Medline
52. Lai, C., Xie, C., McCormack, S. G., Chiang, H. C., Michalak, M. K., Lin, X., Chandran, J., Shim, H., Shimoji, M., Cookson, M. R., Huganir, R. L., Rothstein, J. D., Price, D. L., Wong, P. C., Martin, L. J., Zhu, J. J., and Cai, H. (2006) Amyotrophic lateral sclerosis 2-deficiency leads to neuronal degeneration in amyotrophic lateral sclerosis through altered AMPA receptor trafficking. *J. Neurosci.* **26,** 11798–11806 CrossRef Medline
53. Hsu, F., Spannl, S., Ferguson, C., Hyman, A. A., Parton, R. G., and Zerial, M. (2018) Rab5 and Alsin regulate stress-activated cytoprotective signaling on mitochondria. *Elife* **7,** e32282 CrossRef Medline
54. Taylor, R. C., Acquaah-Mensah, G., Singhal, M., Malhotra, D., and Biswal, S. (2008) Network inference algorithms elucidate Nrf2 regulation of mouse lung oxidative stress. *PLoS Comput. Biol.* **4,** e1000166 CrossRef Medline
55. Suzuki-Utsunomiya, K., Hadano, S., Otomo, A., Kunita, R., Mizumura, H., Osuga, H., and Ikeda, J. E. (2007) ALS2CL, a novel ALS2-interactor, modulates ALS2-mediated endosome dynamics. *Biochem. Biophys. Res. Commun.* **354,** 491–497 CrossRef Medline
56. Mori, Y., Matsui, T., and Fukuda, M. (2013) Rabex-5 protein regulates dendritic localization of small GTPase Rab17 and neurite morphogenesis in hippocampal neurons. *J. Biol. Chem.* **288,** 9835–9847 CrossRef Medline
57. Cirulli, E. T., Lasseigne, B. N., Petrovski, S., Sapp, P. C., Dion, P. A., Leblond, C. S., Couthouis, J., Lu, Y. F., Wang, Q., Krueger, B. J., Ren, Z., Keebler, J., Han, Y., Levy, S. E., Boone, B. E., *et al.* (2015) Exome sequencing in amyotrophic lateral sclerosis identifies risk genes and pathways. *Science* **347,** 1436–1441 CrossRef Medline
58. Farg, M. A., Sundaramoorthy, V., Sultana, J. M., Yang, S., Atkinson, R. A. K., Levina, V., Halloran, M. A., Gleeson, P. A., Blair, I. P., Soo, K. Y., King, A. E., and Atkin, J. D. (2017) C9ORF72, implicated in amytrophic lateral sclerosis and frontotemporal dementia, regulates endosomal trafficking. *Hum. Mol. Genet.* **26,** 4093–4094 CrossRef Medline
59. Shi, Y., Lin, S., Staats, K. A., Li, Y., Chang, W. H., Hung, S. T., Hendricks, E., Linares, G. R., Wang, Y., Son, E. Y., Wen, X., Kisler, K., Wilkinson, B., Menendez, L., Sugawara, T., *et al.* (2018) Haploinsufficiency leads to neurodegeneration in C9ORF72 ALS/FTD human induced motor neurons. *Nat. Med.* **24,** 313–325 CrossRef Medline
60. Fiser, A., and Sali, A. (2003) Modeller: generation and refinement of homology-based protein structure models. *Methods Enzymol.* **374,** 461–491 CrossRef Medline
61. Kyte, J., and Doolittle, R. F. (1982) A simple method for displaying the hydropathic character of a protein. *J. Mol. Biol.* **157,** 105–132 CrossRef Medline
62. Soares, D. C., Barlow, P. N., Porteous, D. J., and Devon, R. S. (2009) An interrupted beta-propeller and protein disorder: structural bioinformatics insights into the N-terminus of alsin. *J. Mol. Model.* **15,** 113–122 CrossRef Medline